Replication stress induces mitotic death through parallel pathways regulated by WAPL and telomere deprotection

V. Pragathi Masamsetti[1], Ka Sin Mak[1], Ronnie Ren Jie Low[1], Chris D. Riffkin[2], Noa Lamm[1], Laure Crabbe[3,4], Jan Karlseder[5], David C.S. Huang[2,6], Makoto T. Hayashi[7] & Anthony J. Cesare[1,8,*]

[1]Children's Medical Research Institute, University of Sydney, Westmead, New South Wales 2145, Australia.

[2]The Walter and Eliza Hall Institute of Medical Research, Parkville, Victoria 3052, Australia.

[3]Institute for Integrative Biology of the Cell (I2BC), CEA, CNRS, Univ. Paris-Sud, Université Paris-Saclay, 91198, Gif-sur-Yvette cedex, France

[4]LBCMCP, Centre de Biologie Intégrative (CBI), Université de Toulouse, CNRS/UPS, Toulouse, France.

[5]The Salk Institute for Biological Studies, Molecular and Cell Biology Department, La Jolla, California 92037, USA.

[6]Department of Medical Biology, The University of Melbourne, Parkville, Victoria 3052, Australia.

[7]Department of Gene Mechanisms, Graduate School of Biostudies/The Hakubi Center for Advanced Research, Kyoto University, Yoshida-Konoe-cho, Sakyo-ku, 606-8501, Japan

[8]Lead contact

*Correspondence: tcesare@cmri.org.au

SUMMARY

Lethal genotoxic stress is associated with "mitotic catastrophe", a broad descriptor encompassing unclear mechanisms of mitotic death. Here we identify that replication stress induces mitotic death through parallel pathways regulated by WAPL and telomere deprotection. We found that lethal replication stress in p53-compromised cells confers spindle assembly checkpoint- and WAPL-dependent mitotic arrest in the same cell cycle. This in turn drives cohesion fatigue and triggers mitotic death through BAX/BAK-mediated intrinsic apoptosis. Simultaneously, another cell death pathway is engaged through non-canonical mitotic telomere deprotection. This minor pathway is regulated by mitotic arrest, TRF2, Aurora B, and ATM, and is independent of telomere length and TRF1. We further identify that suppressing mitotic death promotes genomic instability through diverse mechanisms depending on how cell death is averted. Together these data show that lethal replication stress primarily results in mitotic death and reveal the underlying molecular mechanisms that mediate this lethality.

KEYWORDS

Replication stress, mitotic catastrophe, mitotic death, WAPL, cohesion fatigue, apoptosis, telomeres, telomere deprotection, Aurora B, ATM

INTRODUCTION

Inducing genotoxic or replication stress is a common mechanism of action for frontline chemotherapeutics. Overwhelming a cell's capacity to cope with exogenous DNA damage results in lethality through activation of regulated cell death pathways such as apoptosis or necrosis (Roos et al., 2016). Cell death in response to genotoxic stress is more pronounced in actively dividing cells, which imparts the clinical efficacy of genotoxic agents on proliferative cancers. Consistent with the link between proliferation and cell death, many genotoxic agents are associated with cell death during mitosis (Dominguez-Brauer et al., 2015). Pathways of mitotic death fall under the broad classification of "mitotic catastrophe" (Galluzzi et al., 2018).

Mitotic catastrophe is a regulated onco-suppressive mechanism that responds to aberrant mitoses by removing damaged cells from the cycling population (Vitale et al., 2011). This can occur through cell death or permanent growth arrest after cell division. Whilst mitotic catastrophe has been described for some time, there is no clear understanding of the pathway(s) connecting lethal genotoxic stress to mitotic death (Galluzzi et al., 2018). Nevertheless, evidence suggests that mitotic catastrophe is a mechanism of cell death during chemotherapeutic intervention, and that developing resistance to mitotic catastrophe would impart a selective advantage to neoplastic cells (Denisenko et al., 2016).

Many genotoxic agents directly or indirectly induce "replication stress" (Dobbelstein and Sorensen, 2015). Replication stress is broadly defined as the slowing or inhibition of DNA replication. This includes endogenous stress originating from oncogene expression, repetitive and/or secondary DNA structures, or exogenous stress from pharmacological agents that induce DNA damage, reduce nucleotide production, or inhibit DNA polymerases (Zeman and Cimprich, 2014). Difficulties arising during DNA replication often manifest as mitotic abnormalities, including chromosome segregation errors, anaphase- or ultra-fine bridges, micronuclei, and the passage of replication stress-induced DNA damage through mitosis (Burrell et al., 2013; Chan et al., 2009; Harrigan et al., 2011; Lukas et al., 2011). While replication stress is implicated as a driver of mitotic catastrophe in reviews, there is no established linkage between replication stress and mechanisms of mitotic death.

A connection between DNA replication and mitosis is established through chromosome cohesion. During telophase and early G1, vertebrate Cohesin complexes are loaded onto chromatin (Sumara et al., 2000). The Cohesin antagonist Wings apart-like protein homologue

(WAPL) regulates opening of the Cohesin DNA exit gate to enable dynamic interaction between Cohesin and chromatin (Chan et al., 2012; Kueng et al., 2006). Prior to replication, Cohesin organizes replication origins via chromatin looping to facilitate effective replication in S-phase (Guillou et al., 2010). Coinciding with DNA replication, ECO1 acetylates Cohesin to counteract WAPL activity and establish cohesion until mitosis (Rolef Ben-Shahar et al., 2008; Zhang et al., 2008). In budding yeast, Cohesin associates with stalled replication forks, and Cohesin mobilization promotes the survival of replication stressed cells (Frattini et al., 2017; Tittel-Elmer et al., 2012).

Telomeres, the protective terminal chromosome structures, also have complex functions in DNA replication and mitosis. Canonical telomere function is to mediate chromosome end protection and regulate cell aging as a function of telomere length (Arnoult and Karlseder, 2015). Human cells also possess a length independent non-canonical mitotic telomere function. DNA damage response foci originating during mitotic arrest occur specifically at chromosome ends through a mechanism regulated by the Aurora B kinase, and the telomere protein TRF2 (Hayashi et al., 2012). During mitotic arrest, TRF2 dissociates from chromosome ends resulting in a telomere macromolecular change from telomere-loops (t-loops) to linear telomeres (Hayashi et al., 2012; Van Ly et al., 2018). This exposes the chromosome end as a substrate for the ATM kinase to activate the telomere DNA damage response (DDR)(Van Ly et al., 2018). Telomeres are also repetitive G-rich sequences prone to replication stress, and telomeric DNA replication stress is abrogated through the telomere protein TRF1 (Martinez et al., 2009; Sfeir et al., 2009). How telomere-specific replication stress and/or non-canonical mitotic telomere deprotection impact the cellular response to genomic replication stress are unknown.

Here we investigate the cellular response of human primary and cancer cells to pharmacologically induced DNA replication stress with a specific focus on mitotic catastrophe. We observe that replication stress in p53-competent primary fibroblasts induces mitotic bypass and proliferative arrest. Strikingly, in p53-compromised fibroblasts and cancer cells, we identify that lethal replication-stress confers spindle assembly checkpoint (SAC)-dependent mitotic arrest and mitotic death in the same cell cycle. We find replication stress-induced mitotic death results from parallel pathways. The dominant pathway is regulated by WAPL, which induces unscheduled chromosome segregation during mitotic arrest through “cohesion fatigue” to drive BAX/BAK mediated apoptosis. Depleting WAPL or deleting the essential

mediators of the intrinsic apoptosis pathway (*BAX* and *BAK*), rescued mitotic death at the cost of increased chromosome segregation errors or mitotic slippage. The secondary pathway is signalled through non-canonical mitotic telomere deprotection. Together, we identified new roles for WAPL and for telomeres in sensing replication-stress induced damage and executing mitotic death in response.

RESULTS

Replication stress induces mitotic death

To visualize putative mitotic catastrophe in replication stressed cells, we treated human cells with Aphidicolin (APH) or Hydroxyurea (HU) and visualized the outcomes with live-cell imaging (Movie S1). APH inhibits family B DNA polymerases, whereas HU inhibits ribonucleotide reductase to limit the nucleoside pool available for nascent DNA synthesis. Cultures were visualized after drug treatment with differential interference contrast (DIC) microscopy every six minutes for up to sixty-five hours (Fig. 1A). Mitotic duration was measured from nuclear envelope breakdown to mitotic exit or mitotic death, and mitotic outcomes were classified as normal, mitotic death, multipolar cell division (mitosis resulting in more than two daughter cells), and mitotic slippage (transition from mitosis to interphase without proper cell division) (Fig. 1B).

In primary IMR90 fibroblasts, APH or HU did not impact mitotic duration or mitotic outcome (Fig. 1C, D). Instead, we observed a marked reduction in mitotic entry consistent with proliferative arrest (Fig. 1E, S1A). In contrast, IMR90 cells with p53 and Rb inhibited through exogenous expression of HPV16 E6 and E7 (IMR90 E6E7) showed a significant increase in mitotic duration and mitotic death with escalating dosages of APH and HU (Fig. 1C, D). Two-dimensional data representation revealed that mitoses leading to cell death arose after 20 hours of APH or HU treatment, and that mitotic death correlated with increased mitotic duration (Fig. 1F, S1A). IMR90-hTERT cultures expressing the dominant negative p53DD allele also depicted similar mitotic arrest and mitotic death with delayed kinetics in response to lethal APH, indicating that p53 inhibition is necessary to enable mitotic death in response to replication stress (Fig. S1B, C).

p53-compromised cancer cells exhibited similar replication stress-induced mitotic arrest and death. HT1080 6TG cells are a p53 mutant derivative of the HT1080 fibrosarcoma cell line.

Treating HT1080 6TG cells with escalating concentrations of APH and HU revealed concomitant significant increases in mitotic duration and mitotic death (Fig. 1G, H). Mitotic events resulting in cell death started 20 hours after 1 μM APH, or 30 hours after 500 μM HU treatment, with mitotic death correlating with increased mitotic duration (Fig. 1I, S1D). HeLa cervical carcinoma cells and p53-null Saos-2 osteosarcoma cells also exhibited increased mitotic duration and mitotic death when treated with lethal dosages of APH (Fig. S1E, F).

Lethal replication stress induces SAC-dependent mitotic arrest

Correlation observed between mitotic duration and mitotic death suggests that mitotic arrest drives replication stress induced lethality. The spindle assembly checkpoint (SAC) is regulated by MPS1 kinase and arrests mitosis until tension is established across the mitotic spindle (Musacchio, 2015). We tested SAC involvement in replication stress-induced mitotic arrest by performing live cell imaging in cultures treated with APH or HU, and the MPS1 inhibitor Reversine (Santaguida et al., 2010). Reversine suppressed both mitotic arrest and mitotic death, consistent with mitotic arrest being a key determinant of lethality (Fig. 1J-L, S1G). Additionally, Reversine rescue of mitotic death conferred an increase in multipolar cell division in APH treated cells and mitotic slippage in HU treated cultures (Fig. 1K).

Replication stress induces mitotic death in the same cell cycle

Mitotic death in p53-compromised cells required twenty or more hours of APH or HU treatment. To determine if replication stress and mitotic lethality occurred in the same cell cycle, we created HT1080 6TG cultures stably expressing the colorimetric *f*luorescent, *u*biquitination-based *c*ell *c*ycle *i*ndicator (FUCCI) system (Sakaue-Sawano et al., 2008) (Fig. 2A). FUCCI cultures were visualized with DIC and fluorescent live cell imaging every six minutes for up to sixty hours (Movie S2). Cells were scored during their first cell cycle after APH or DMSO treatment, with G1 and S/G2 phases determined, respectively, by mCherry-hCdt1(30/120) and mVenus-hGeminin(1/110) stability. Mitotic duration and outcomes were classified as described above, with the addition of mitotic bypass, defined as transition from G2 [mVenus-hGeminin(1/110) expressing] to G1-phase [mCherry-hCdt1(30/120) expressing] without mitotic entry (Fig. 2A). We also scored for interphase cell death (Fig. 2A).

HT1080 6TG-FUCCI cells displayed a stratified response characterized by cell cycle phase at the time of APH treatment. We observed that cells already in S/G2, which remained there for < 20 hours with APH treatment, displayed little to no mitotic arrest or cell death phenotype

(Fig. 2B, C). While cells already in S/G2, and which remained there for > 20 hours with APH treatment, displayed common subsequent mitotic arrest and mitotic death in the same cell cycle (Fig 2B, C). APH did not impact G1 duration (Fig. 2D). However, cells in G1 when APH was administered displayed a subsequent extended S/G2, mitotic arrest and mitotic death all in the same cell cycle (Fig. 2B, D). Notably, 85% of cell death in HT1080 6TG-FUCCI cells observed in the first cell cycle with APH treatment occurred during mitosis (Fig. 2E).

To determine if persistent APH treatment during cell division impacted mitotic arrest and mitotic death, we imaged HT1080 6TG-FUCCI cells following APH treatment and washout of the drug from the growth media. For these experiments, cells were cultured with 1 μM APH for 30 hours before media washout and replacement with culture media containing DMSO or fresh 1 μM APH (Fig. S2A, B). We observed that APH washout failed to rescue lethality in cells arrested in mitosis. Additionally, for two hours after APH removal, cells continued to enter mitosis, arrest and die. Mitotic arrest thus did not result from persistent APH treatment during cell division. This indicates instead that a phenotype induced by lethal replication stress, when passed into mitosis, is sufficient to confer mitotic arrest and death.

p53 competent fibroblasts bypass mitosis in response to replication stress

To determine how replication stress impacted proliferative dynamics in p53-competent primary fibroblasts, we live-cell imaged IMR90 FUCCI cultures. APH treatment of p53-competent IMR90-FUCCI cells induced an extended S/G2, mitotic bypass, and a subsequent G1-phase growth arrest (Fig. S2C). In cells that bypassed mitosis, we did not observe subsequent S-phase re-entry or cell division. This observation is consistent with previous results identifying that p53-activation from a genomic DDR is sufficient to induce mitotic bypass and proliferative arrest (Johmura et al., 2014; Krenning et al., 2014). We note that IMR90 FUCCI cells in G1 at the time of APH addition often displayed what appeared as sustained G1-arrest without S-phase entry (Fig. S2C). This likely reflects arrest in early S-phase when mCherry-hCdt1(30/120) remains stable. p53 therefore limits cellular proliferation following replication stress by inducing sustained growth arrest either without DNA synthesis or after mitotic bypass. For the remainder of this study we focused on mitotic death in p53-compromised cells.

Distinct types of mitotic death are induced by replication stress

The specific contribution of cell death pathways in mitotic catastrophe is poorly understood (Galluzzi et al., 2018). BAX and BAK are BCL-2 family proteins essential for apoptosis

through their role in mitochondrial outer membrane permeabilization (Czabotar et al., 2014; Wei et al., 2001). Using CRISPR-Cas9 we generated clonal HeLa and HT1080 6TG *BAX* and *BAK* double knock out (*BAX BAK* DKO) cell lines (Fig. S3A). Parental and *BAX BAK* DKO cells were treated with APH and visualized with live cell imaging. APH induced mitotic arrest in *BAX BAK* DKO cultures, with individual mitotic events exhibiting a longer duration mitotic arrest than observed in parental cells (Fig 3A, B, S3B-D). Significantly, *BAX BAK* DKO rescued most, but not all, mitotic death events in APH treated cells (Fig. 3C, S3E). This reduced lethality was accompanied with an increase in multipolar cell division and mitotic slippage (Fig. 3C, S3E).

Observation of apoptosis-dependent and -independent mitotic lethality suggested the potential for multiple mitotic death initiating events in response to replication stress. To visualize this possibility, we live-cell imaged HT1080 6TG H2B-mCherry cells treated with a lethal dose of APH. These experiments revealed two chromosome phenotypes associated with mitotic death (Fig. 3D, Movie S3). “Type 1” mitotic death was defined by a dispersion of chromosomal material immediately preceding lethality, whereas “Type 2” mitotic death was defined by the collapse or condensation of the genetic material without chromosome dispersion (Fig. 3D). Type 1 mitotic death was the dominant outcome, contributing 69.5 ± 1.9% (mean ± s.e.m.) of total cell death events, while Type 2 mitotic death accounted for 23.5 ± 1.2% of cell lethality, with the remaining 7.0 ± 2.3% of cell death occurring during interphase (Fig. 3E).

Lethal replication stress induces cohesion fatigue

We characterized the mitotic chromosome phenotypes associated with mitotic death by preparing fixed samples using standard cytogenetic chromosome preparations. Samples were stained with centromere and telomere fluorescent in situ hybridization (FISH) to orient chromosome morphology (Fig. 4A, B). This revealed a major phenotype of aberrant chromosome cohesion. We sub-classified the cohesion abnormalities as a “mild” phenotype defined by visible separation of sister centromeres; a “moderate” phenotype of cohesion loss between sister centromeres and the adjacent chromosomal region, with cohesion remaining at distal chromosome arms; and a “severe” phenotype of complete sister chromatid separation (Fig. 4B). Replication stress also induced entangled chromosomes, consistent with condensation defects induced by replication stress (Figure S4A)(Lamm et al., 2016).

Quantitation of HT1080 6TG cells treated with 1 μM APH or 350 μM HU identified that both conditions induced significant increases in the mild, moderate and severe cohesion phenotype (Fig 4C, S4B). Notably, the mild and moderate cohesion phenotypes initiated from the centromeres (Fig. 4B), suggesting involvement of microtubule pulling forces driving chromatid separation through exertion on the kinetochores. To test this, we treated cells with a lethal dose of APH or HU in combination with Colcemid or Taxol to inhibit microtubule dynamics, or Reversine to silence the SAC (Fig. 4A). In APH and HU treated cells, Taxol, Colcemid, and Reversine all suppressed the moderate and severe cohesion phenotype (Fig. 4C, S4B). These observations are consistent with "cohesion fatigue", a phenomena where sustained microtubule pulling forces exerted during mitotic arrest drive unscheduled chromosome segregation prior to anaphase onset (Daum et al., 2011; Sapkota et al., 2018). We interpret these data to indicate the moderate and severe conditions represent a phenotypic continuum of cohesion fatigue as sister chromatids are progressively separated during mitotic arrest. Conversely, the mild cohesion phenotype was not impacted by Reversine, Taxol or Colcemid, indicating its dependence on replication stress, but neither mitotic arrest nor microtubule-dependent tensional force. Chromosome entanglement occurred in all replication stress conditions (Fig. 4C, S4A, B)(Lamm et al., 2016). However, the complexity of entangled chromosomes prevented classification of cohesion status and was thus excluded from subsequent quantitative analysis.

Type 1 mitotic death is dependent on WAPL and BAX/BAK-driven apoptosis

WAPL depletion was previously shown to increase Cohesin retention on chromatin and suppress cohesion fatigue (Daum et al., 2011; Gandhi et al., 2006; Kueng et al., 2006). To probe for WAPL involvement in the replication stress-induced cohesion phenotypes, we siRNA depleted WAPL and treated cultures with a lethal dose of APH or HU (Fig. 4D, E). Chromosome cohesion phenotypes were measured in cytogenetic chromosome preparations, and mitotic duration and outcome by live-cell imaging (Fig. 4F-I, S5A-F).

WAPL depletion suppressed the mild, moderate and severe sister chromatid cohesion phenotypes induced by APH and HU in HT1080 6TG cells (Fig. 4F-G, S5A). Additionally, WAPL depletion substantially reduced mitotic duration and rescued mitotic death in HT1080 6TG cultures treated with 1 μM APH or 350 μM HU (Fig 4H-I, S4B-C). This was not an artefact of reduced cell proliferation, as APH and HU treated cells continued to enter mitosis in WAPL depleted cultures (Fig. S5D). WAPL depletion also significantly reduced mitotic

duration and mitotic death in 1 μM APH treated HeLa cultures at the cost of a significant increase in multipolar cell divisions (Fig. S5E, F).

As WAPL depletion and *BAX BAK* DKO both rescued most of the mitotic death induced by replication stress, we reasoned that WAPL and BAX/BAK functioned in the same pathway. To test this, we created HT1080 6TG H2B-mCherry *BAX BAK* DKO cells (Fig. S5G). We then treated HT1080 6TG H2B-mCherry, WAPL depleted HT1080 6TG H2B-mCherry, or HT1080 6TG H2B-mCherry *BAX BAK* DKO cells with 1 μM APH and visualized mitotic outcomes with live cell imaging (Fig. 4J-K, S5H). WAPL depletion completely suppressed Type 1 mitotic death with no significant effect on Type 2 mitotic or interphase death (Fig. 4K). Similarly, *BAX BAK* DKO also largely suppressed Type 1 mitotic death with no significant effect on Type 2 mitotic or interphase death (Fig. 4K). Together the data indicate WAPL and BAX/BAK regulate Type 1 mitotic death in response to lethal replication stress.

We also quantified how suppressing mitotic death by WAPL depletion or *BAX BAK* DKO impacted genome stability. In the absence of replication stress, WAPL depletion induced a slight but significant increase in chromosome segregation errors in HT1080 6TG H2B-mCherry cells (6.0% ± 2.4 of mitoses resulting in micronuclei or multipolar cell division, mean ± s.e.m., Fig. S5H). However, when combined with 1 μM APH, WAPL depletion conferred a sharp increase in multipolar cell division or mitoses resulting in micronuclei formation (47.2% ± 2.8 of mitotic events, Fig. 4J,K). Alternatively, APH treatment in HT1080 6TG H2B-mCherry *BAX BAK* DKO cells did not increase chromosomal segregation errors, but instead induced a significant increase in mitotic slippage (Fig. 4J,K).

Lethal replication stress induces non-canonical mitotic telomere deprotection

To address potential mechanisms contributing to Type 2 mitotic death, we assayed DDR activation on cytocentrifuged mitotic chromatin following treatment with lethal dosages of APH or HU (Fig. 5A, B). Surprisingly, we observed similar numbers of genomic and telomeric γ-H2AX foci on mitotic chromosomes from APH and HU treated cells (Fig. 5C). Because telomeres represent a minor proportion of the total genome, this suggested a telomere-specific phenotype accompanying lethal replication stress. One possibility is that exogenous replication stress disproportionally affects the difficult to replicate telomeric DNA (Crabbe et al., 2004; Miller et al., 2006; Sfeir et al., 2009). Replication stress in vertebrate telomeres is attenuated through the telomere-specific TRF1 protein (Sfeir et al., 2009).

To investigate putative contribution of telomere-specific replication stress in mitotic lethality, we over-expressed mCherry-TRF1 (mCherry-TRF1^{OE}) in HT1080 6TG cells (Fig. 5D). mCherry-TRF1^{OE} failed to reduce the number of mitotic telomere DDR foci observed with APH treatment (Fig. 5E, F). mCherry-TRF1^{OE} also failed to impact mitotic duration or confer a survival advantage to cells treated with 1 μM APH (Fig. 5G, H), indicating mitotic outcomes observed with lethal APH treatment are independent of replication stress in the telomeric DNA.

Alternatively, the mitotic telomere DDR observed with lethal replication stress could arise from non-canonical mitotic telomere deprotection (Fig S6A)(Hayashi et al., 2012). To test this, we treated HT1080 6TG cells with lethal dosages of APH or HU in combination with the SAC inhibitor Reversine, the Aurora B inhibitor Hesperadin, or the ATM inhibitor KU-55933 (Fig. 5I,J)(Hauf et al., 2003; Hickson et al., 2004). Consistent with non-canonical mitotic telomere deprotection, the telomere DDR observed with lethal APH or HU was significantly suppressed by inhibiting Aurora B, ATM, or mitotic arrest with Reversine (Fig 5J, S6B). Conversely, Reversine and Hesperadin did not reduce the genomic DDR induced by APH or HU, indicating the reduced load of telomeric γ-H2AX foci did not result from global DDR suppression (Fig. 5I, S6B). KU-55933 treatment did reduce genomic DDR foci induced by APH or HU, consistent with the global role for ATM in DDR signalling. Additionally, measurement of telomere FISH signal intensity as a readout of telomere length revealed the mitotic telomere DDR induced with 1 μM APH did not associate with telomere shortening (Fig. 5K), consistent with length independent non-canonical mitotic telomere deprotection (Hayashi et al., 2012). Mitotic telomere deprotection did occur in parallel with cohesion fatigue as demonstrated by DDR-positive telomeres in mitoses with separated sister chromatids (Fig. S6C).

Mitotic telomere deprotection contributes to replication stress lethality

Non-canonical mitotic telomere deprotection is regulated by TRF2 (Hayashi et al., 2012). While *TRF2* deletion results in the total loss of telomere protection and end-to-end chromosome fusions (Celli and de Lange, 2005), partial TRF2 depletion induces "intermediate-state" telomeres that activate the ATM-dependent DDR but still suppress covalent telomere fusion (Cesare et al., 2013; Cesare et al., 2009). Expression of TRF2 shRNAs of differing efficiency in HT1080 6TG cells was previously shown to induce only intermediate-state telomeres (TRF2 sh-F), or both intermediate-state telomeres and end-to-end chromosome fusions (TRF2 sh-G) (Cesare et al., 2013). Additionally, TRF2 depletion and over-expression

(TRF2^{OE}) were previously shown to respectively sensitize and suppress non-canonical mitotic telomere deprotection (Hayashi et al., 2012).

To test if mitotic telomere deprotection impacts replication stress-induced mitotic lethality, we created HT1080 6TG TRF2 sh-F and HT1080 6TG TRF2^{OE} cell lines (Fig. 6A). Cell line characterization identified that TRF2^{OE} and TRF2 sh-F had no impact on genomic DNA replication rates (S7A, B), and that manipulating TRF2 expression did not impact cohesion fatigue induced by replication stress (Fig. S7C). Furthermore, TRF2 sh-F did not induce covalent telomere-telomere fusions as a potential source of mitotic arrest (Hayashi et al., 2015) (Fig. S7D-F). We then treated HT1080 6TG TRF2 sh-F or TRF2^{OE} cells with 1 μM APH and assayed telomere deprotection on cytocentrifuged chromosome spreads, and mitotic outcomes using live cell imaging (Fig. 6B-G, S7G).

Consistent with previous observations, TRF2 sh-F induced a telomere-specific DDR in the absence of replication stress (Fig. 6C)(Cesare et al., 2013). However, in conjunction with 1 μM APH, TRF2 sh-F significantly exacerbated the mitotic telomere deprotection phenotype (Fig. 6C, E). Conversely, TRF2^{OE} suppressed mitotic telomere deprotection in 1 μM APH treated cells (Fig. 6D, E). TRF2 sh-F and TRF2^{OE} had either an insignificant or very modest impact on mitotic duration with 1 μM APH treatment (Fig. S7G). However, TRF2 sh-F significantly reduced the duration of mitotic arrest until cell death in response to 1 μM APH (Fig. 6F). TRF2 sh-F also induced a small but significant increase in mitotic death in cells treated with 1 μM APH, whereas TRF2^{OE} conferred a small but significant suppression of mitotic death with the same dose of replication stress (Fig. 6G). Cumulatively the data are consistent with mitotic telomere deprotection contributing to a minor proportion of mitotic lethality in response to lethal replication stress.

DISCUSSION

Here we identify that lethal replication stress induces mitotic death and define novel roles for WAPL and telomeres in regulating cell lethality (Fig. 7). We found that replication stress induced proliferative arrest in p53 competent fibroblasts by preventing DNA synthesis, or through mitotic bypass. Conversely, lethal replication stress in p53-compromised human fibroblasts and cancer cells induced SAC-dependent mitotic arrest in the same cell cycle. Sustained mitotic arrest conferred mitotic death through a primary Type 1 pathway dependent on WAPL and mitochondrial apoptosis driven by BAX/BAK. Non-canonical telomere

deprotection also contributed to a secondary pathway of mitotic death. Suppressing the SAC, WAPL or BAX/BAK rescued mitotic lethality at the cost of genome instability. As many frontline chemotherapeutics directly or indirectly induce replication stress (Dobbelstein and Sorensen, 2015), these findings provide insight into mechanisms that confer resistance to chemotherapeutics and propagate cancer evolution.

Replication stress induces mitotic catastrophe

We found that lethal replication stress induced a striking phenotype of mitotic arrest and mitotic death in p53-compromised human cells. This was consistent across multiple cell lines where greater than 80% of replication stress lethality occurred during mitosis. Cells in G1-phase when treated with APH, or cells in S/G2 that subsequently took greater than 20 hours to enter mitosis, had the highest incidence of mitotic death. We interpret these data to indicate that encountering replication stress in early S-phase corresponded with the greatest probability for mitotic lethality. Notably, lethal replication stress conferred mitotic death in the same cell cycle: signifying that mitotic death is an active process to eliminate compromised cells in the immediate mitosis, as opposed to knock-on effect resulting from genomic instability accumulated over multiple cell cycles. Our data also identify a critical role for the SAC in regulating replication stress lethality through its role in maintaining mitotic arrest.

Replication stress is repaired in part during mitosis through a mechanism dependent POLD3, a component of the DNA polymerase δ complex that is inhibited by APH. (Bhowmick et al., 2016; Byrnes, 1984; Minocherhomji et al., 2015). However, APH washout failed to rescue the arrest of cells in mitosis, or those cells entering mitosis in the following two hours. Mitotic arrest therefore does not result from inhibiting mitotic DNA synthesis. We interpret these data to indicate instead that a phenotype induced by replication stress prior to mitotic entry confers mitotic arrest. We suggest this is linked to the minor cohesion loss phenotype. In contrast to the moderate and severe phenotypes, the mild cohesion phenotype was dependent on replication stress but not mitotic arrest nor microtubule dynamics. Failure to establish or maintain cohesion at sister centromeres likely impacts the kinetochores, or spindle tension, to maintain the SAC. In agreement, mitotic arrest was conferred when centromeric cohesion was impaired by alternative methods (Salic et al., 2004; Tang et al., 2004), and WAPL depletion co-rescued both mitotic arrest and the minor cohesion phenotype in APH or HU treated cells.

Replication stress induces parallel mechanisms of mitotic death

We also observed that replication stress induced distinct mechanisms of mitotic death. The major Type 1 mechanism was defined by chromosome dispersion via WAPL-dependent cohesion fatigue. Depleting WAPL or *BAX BAK* DKO both suppressed Type 1 mitotic death, connecting replication stress-induced cohesion fatigue to intrinsic apoptosis. Cytogenetically, we observed that the majority of chromosomes in a mitotic cell typically displayed similar cohesion phenotypes. This suggests that cohesion fatigue progresses uniformly on most chromosomes during replication stress-induced mitotic arrest. We were unable to identify how cohesion fatigue signals apoptosis. However, one intriguing possibility is that sudden loss of spindle tension on multiple chromosomes induces signalling to activate the apoptotic cascade. Because cohesion fatigue requires microtubule pulling forces, it is important to note that mitotic death induced by replication stress may differ mechanistically from mitotic death in cells treated with poisons that inhibit microtubule dynamics.

The minor Type 2 mechanism was defined by a lack of chromosome dispersion before lethality. Several lines of evidence connect mitotic telomere deprotection to Type 2 mitotic death, and indicate that telomere deprotection and cohesion fatigue progress independently during mitotic arrest. Specifically, WAPL depletion imparted no significant impact on Type 2 mitotic death. Additionally, augmenting telomere protection through TRF2 overexpression or depletion suppressed or promoted mitotic death without affecting centromere cohesion. Further, the subtle effect on mitotic death by altering TRF2 expression is consistent with telomeres functioning in the minor Type 2 pathway. While we conclude telomeres contribute to Type 2 cell death, we cannot exclude the participation of other factors.

Our interpretation is that cohesion fatigue and telomere deprotection occur in parallel during mitotic arrest. This was supported by our observation of DDR-positive telomeres in cytocentrifuged mitotic spreads with completely separated sister chromatids. We suggest mitotic death occurs when either cohesion fatigue or telomere deprotection reaches a signalling threshold within an individual mitosis. Amplifying telomere deprotection with a TRF2 shRNA thus shortens mitotic duration to cell death as the aggregate signalling from deprotected telomeres increases. However, $TRF2^{OE}$ did not extend mitotic duration, as cohesion fatigue remained active to induce lethality. Conversely, telomere deprotection could enable cell death independent of apoptosis in *BAX BAK* DKO cells.

WAPL mediates mitotic arrest and death

A significant finding in our study is that WAPL plays a major role mediating replication stress-induced cell death. A straightforward explanation is that WAPL drives cohesion fatigue during mitotic arrest to induce mitotic lethality (Daum et al., 2011). This, however, is likely an over-simplification of WAPL function. Cohesin dynamically interacts with chromatin and stalled replication forks (Tittel-Elmer et al., 2012). Further, inhibiting WAPL-dependent Cohesin mobilization impacts cell viability in budding yeast treated with replication stress inducing drugs (Frattini et al., 2017). WAPL also regulates three-dimensional genome architecture though chromatin looping (Busslinger et al., 2017; Haarhuis et al., 2017; Tedeschi et al., 2013; Wutz et al., 2017), and chromatin looping organizes replication origins to facilitate effective DNA replication (Guillou et al., 2010). Consistent with WAPL playing a more expansive role in regulating lethality, we observed that WAPL depletion also suppressed both the minor cohesion phenotype and mitotic arrest in APH and HU treated cells. WAPL therefore regulates centromeric cohesion in response to replication stress as a putative mechanism to drive SAC-dependent mitotic arrest. Future studies will focus on determining how WAPL cooperates with replication stress to confer mitotic arrest, potentially through its interaction with Cohesin regulators at centromeres and its control over chromatin architecture.

Telomeres contribute to replication stress-induced mitotic death

We also identified that lethal replication stress induced telomere-specific DDR signalling. Surprisingly, we found the mitotic telomere DDR induced by replication stress was resistant to over-expression of the telomere replication regulator TRF1. Instead, we found the telomere DDR stemmed from activation of non-canonical mitotic telomere deprotection regulated by mitotic arrest, Aurora B, ATM, and TRF2 (Hayashi et al., 2012). Telomeres inhibit ATM through sequestration of the chromosome terminus within a t-loop (Van Ly et al., 2018). ATM activation at chromosome ends occurs with the macromolecular structural change from looped to linear telomeres, through exposure of the chromosome terminus as an ATM activating substrate (Van Ly et al., 2018). We interpret these data to indicate that human chromosome ends actively signal replication stress-induced mitotic distress by changing telomere structure to activate the ATM-dependent DDR. We have thus demonstrated a novel mechanism where telomeres contribute to overall genome stability by eliminating replication stressed cells from the cycling population.

Evading mitotic death leads to genome instability

Evading mitotic catastrophe will confer a growth advantage to neoplastic cells (Dominguez-Brauer et al., 2015). We showed that suppressing Type 1 mitotic death by inhibiting intrinsic apoptosis resulted in mitotic slippage, while WAPL depletion substantially elevated chromosome segregation errors. Both of these outcomes result in supernumerary chromosomes, which induces p53-dependent growth arrest in healthy tissues (Thompson and Compton, 2010). However, we found p53 inhibition was requisite for mitotic entry in replication stressed cells. Mutations that confer evasion of mitotic death in p53-compromised cells are thus likely to also propagate chromosomal instability, thus driving tumour heterogeneity and cancer evolution (Sansregret and Swanton, 2017). Chromosome segregation errors occurring with mitotic catastrophe rescue may also activate the cGAS-STING pathway to drive metastasis (Bakhoum et al., 2018; Harding et al., 2017). WAPL mutations are observed in cancers, but occur at a lower frequency than mutations in other Cohesin subunits (Hill et al., 2016). Notably, the STAG2 Cohesin subunit is commonly mutated in human malignancies, and patient derived *STAG2* mutations were found to confer reduced interaction of the STAG2 and WAPL proteins (Hill et al., 2016). It will be interesting in the future to determine if mutations in WAPL or its regulatory partners confer resistance to replication stress-inducing chemotherapeutics and if this has potential clinical value in cancer stratification. Cumulatively, this study identifies that lethal replication stress primarily results in mitotic death and reveals the underlying mechanism driving this type of mitotic catastrophe.

ACKNOWLEDGEMENTS

All data are archived at the Children's Medical Research Institute (CMRI), Kyoto University, or the Walter and Eliza Hall institute of Medical Research (WEHI). Scott Page and the CMRI ACRF Telomere Analysis Centre, supported by the Australian Cancer Research Foundation, are thanked for microscopy infrastructure. Leszek Lisowski is thanked for generating viral vectors at the Salk Institute's GT3 Core and CMRI's Vector and Genome Engineering Facility. The Salk Institute's Flow Cytometry Core is thanked for assistance with cell sorting. V.P.M. is supported by an Australian Post-Graduate Award from the University of Sydney. N.L. is supported by fellowships from the Hebrew University Smorgon Foundation and the Cancer Institute NSW. L.C. is supported by the ATIP starting grant from CNRS in the framework of Plan Cancer 2014-2019, the ANR Tremplin ERC (55911) and the European Research Council grant teloHOOK/ERC (714653). J.K. is supported by The NIH (R01GM087476, R01CA174942), the Donald and Darlene Shiley Chair, the Highland Street Foundation, the Fritz B. Burns Foundation, the Emerald Foundation and the Glenn Center for Aging Research. Work in the laboratory of D.C.S.H is supported by fellowships and grants from the Australian NHMRC (1043149, 1016701, 1113133), Leukemia Lymphoma Society SCOR (11283-17), Independent Research Institutes Infrastructure Support Scheme grant (9000220) and a Victorian State Government Operational Infrastructure Support (OIS) grant. M.T.H. is supported by grants from the Senri Life Science Foundation, the Uehara Memorial Foundation, the Daiichi Sankyo Foundation of Life Science, the Nakajima Foundation, The Mochida Memorial Foundation Research Grant, Grant-in-Aid for Young Scientists (A) (16H06176) and Grant-in-Aid for Scientific Research on Innovative Areas (16H01406). A.J.C. is supported by grants from the Australian NHMRC (1053195, 1106241, 1104461), the Cancer Council NSW (RG 15-12), the Cancer Institute NSW (11/FRL/5-02) and philanthropy from Stanford Brown, Inc (Sydney, Australia).

AUTHOR CONTRIBUTIONS

V.P.M., J.K., D.C.S.H., M.T.H. and A.J.C. conceived the study and designed experiments. V.P.M, K.S.M., R.R.J.L., C.D.R., N.L., L.C. and M.T.H. performed experiments. V.P.M. and A.J.C. wrote the manuscript with editorial assistance from J.K., D.C.S.H., and M.T.H.

DECLARATION OF INTERESTS

The authors declare no competing interests.

REFERENCES

Arnoult, N., and Karlseder, J. (2015). Complex interactions between the DNA-damage response and mammalian telomeres. Nature structural & molecular biology *22*, 859-866.

Bakhoum, S.F., Ngo, B., Laughney, A.M., Cavallo, J.A., Murphy, C.J., Ly, P., Shah, P., Sriram, R.K., Watkins, T.B.K., Taunk, N.K., *et al.* (2018). Chromosomal instability drives metastasis through a cytosolic DNA response. Nature *553*, 467-472.

Bhowmick, R., Minocherhomji, S., and Hickson, I.D. (2016). RAD52 Facilitates Mitotic DNA Synthesis Following Replication Stress. Molecular cell *64*, 1117-1126.

Burrell, R.A., McClelland, S.E., Endesfelder, D., Groth, P., Weller, M.C., Shaikh, N., Domingo, E., Kanu, N., Dewhurst, S.M., Gronroos, E., *et al.* (2013). Replication stress links structural and numerical cancer chromosomal instability. Nature *494*, 492-496.

Busslinger, G.A., Stocsits, R.R., van der Lelij, P., Axelsson, E., Tedeschi, A., Galjart, N., and Peters, J.M. (2017). Cohesin is positioned in mammalian genomes by transcription, CTCF and Wapl. Nature *544*, 503-507.

Byrnes, J.J. (1984). Structural and functional properties of DNA polymerase delta from rabbit bone marrow. Molecular and cellular biochemistry *62*, 13-24.

Celli, G.B., and de Lange, T. (2005). DNA processing is not required for ATM-mediated telomere damage response after TRF2 deletion. Nature cell biology *7*, 712-718.

Cesare, A.J., Hayashi, M.T., Crabbe, L., and Karlseder, J. (2013). The telomere deprotection response is functionally distinct from the genomic DNA damage response. Molecular cell *51*, 141-155.

Cesare, A.J., Heaphy, C.M., and O'Sullivan, R.J. (2015). Visualization of Telomere Integrity and Function In Vitro and In Vivo Using Immunofluorescence Techniques. Current protocols in cytometry / editorial board, J. Paul Robinson, managing editor ... [et al *73*, 12 40 11-31.

Cesare, A.J., Kaul, Z., Cohen, S.B., Napier, C.E., Pickett, H.A., Neumann, A.A., and Reddel, R.R. (2009). Spontaneous occurrence of telomeric DNA damage response in the absence of chromosome fusions. Nature structural & molecular biology *16*, 1244-1251.

Chan, K.L., Palmai-Pallag, T., Ying, S., and Hickson, I.D. (2009). Replication stress induces sister-chromatid bridging at fragile site loci in mitosis. Nature cell biology *11*, 753-760.

Chan, K.L., Roig, M.B., Hu, B., Beckouët, F., Metson, J., and Nasmyth, K. (2012). Cohesin's DNA exit gate is distinct from its entrance gate and is regulated by acetylation. Cell *150*, 961-974.

Crabbe, L., Cesare, A.J., Kasuboski, J.M., Fitzpatrick, J.A., and Karlseder, J. (2012). Human telomeres are tethered to the nuclear envelope during postmitotic nuclear assembly. Cell reports *2*, 1521-1529.

Crabbe, L., Verdun, R.E., Haggblom, C.I., and Karlseder, J. (2004). Defective telomere lagging strand synthesis in cells lacking WRN helicase activity. Science (New York, N.Y *306*, 1951-1953.

Czabotar, P.E., Lessene, G., Strasser, A., and Adams, J.M. (2014). Control of apoptosis by the BCL-2 protein family: implications for physiology and therapy. Nature reviews *15*, 49-63.

Daum, J.R., Potapova, T.A., Sivakumar, S., Daniel, J.J., Flynn, J.N., Rankin, S., and Gorbsky, G.J. (2011). Cohesion fatigue induces chromatid separation in cells delayed at metaphase. Curr Biol *21*, 1018-1024.

Denisenko, T.V., Sorokina, I.V., Gogvadze, V., and Zhivotovsky, B. (2016). Mitotic catastrophe and cancer drug resistance: A link that must to be broken. Drug Resist Updat *24*, 1-12.

Dobbelstein, M., and Sorensen, C.S. (2015). Exploiting replicative stress to treat cancer. Nature reviews *14*, 405-423.

Dominguez-Brauer, C., Thu, K.L., Mason, J.M., Blaser, H., Bray, M.R., and Mak, T.W. (2015). Targeting Mitosis in Cancer: Emerging Strategies. Molecular cell *60*, 524-536.

Frattini, C., Villa-Hernández, S., Pellicanò, G., Jossen, R., Katou, Y., Shirahige, K., and Bermejo, R. (2017). Cohesin Ubiquitylation and Mobilization Facilitate Stalled Replication Fork Dynamics. Molecular cell *68*, 758-772.e754.

Galluzzi, L., Vitale, I., Aaronson, S.A., Abrams, J.M., Adam, D., Agostinis, P., Alnemri, E.S., Altucci, L., Amelio, I., Andrews, D.W.*, et al.* (2018). Molecular mechanisms of cell death: recommendations of the Nomenclature Committee on Cell Death 2018. Cell Death & Differentiation *25*, 486-541.

Gandhi, R., Gillespie, P.J., and Hirano, T. (2006). Human Wapl is a cohesin-binding protein that promotes sister-chromatid resolution in mitotic prophase. Curr Biol *16*, 2406-2417.

Guillou, E., Ibarra, A., Coulon, V., Casado-Vela, J., Rico, D., Casal, I., Schwob, E., Losada, A., and Méndez, J. (2010). Cohesin organizes chromatin loops at DNA replication factories. Genes and Development *24*, 2812-2822.

Haarhuis, J.H.I., van der Weide, R.H., Blomen, V.A., Yáñez-Cuna, J.O., Amendola, M., van Ruiten, M.S., Krijger, P.H.L., Teunissen, H., Medema, R.H., van Steensel, B.*, et al.* (2017). The Cohesin Release Factor WAPL Restricts Chromatin Loop Extension. Cell *169*, 693-707.e614.

Harding, S.M., Benci, J.L., Irianto, J., Discher, D.E., Minn, A.J., and Greenberg, R.A. (2017). Mitotic progression following DNA damage enables pattern recognition within micronuclei. Nature *548*, 466-470.

Harrigan, J.A., Belotserkovskaya, R., Coates, J., Dimitrova, D.S., Polo, S.E., Bradshaw, C.R., Fraser, P., and Jackson, S.P. (2011). Replication stress induces 53BP1-containing OPT domains in G1 cells. The Journal of cell biology *193*, 97-108.

Hauf, S., Cole, R.W., LaTerra, S., Zimmer, C., Schnapp, G., Walter, R., Heckel, A., van Meel, J., Rieder, C.L., and Peters, J.M. (2003). The small molecule Hesperadin reveals a role for Aurora B in correcting kinetochore-microtubule attachment and in maintaining the spindle assembly checkpoint. The Journal of cell biology *161*, 281-294.

Hayashi, M.T., Cesare, A.J., Fitzpatrick, J.A., Lazzerini-Denchi, E., and Karlseder, J. (2012). A telomere-dependent DNA damage checkpoint induced by prolonged mitotic arrest. Nature structural & molecular biology *19*, 387-394.

Hayashi, M.T., Cesare, A.J., Rivera, T., and Karlseder, J. (2015). Cell death during crisis is mediated by mitotic telomere deprotection. Nature *522*, 492-496.

Hickson, I., Zhao, Y., Richardson, C.J., Green, S.J., Martin, N.M., Orr, A.I., Reaper, P.M., Jackson, S.P., Curtin, N.J., and Smith, G.C. (2004). Identification and characterization of a novel and specific inhibitor of the ataxia-telangiectasia mutated kinase ATM. Cancer research *64*, 9152-9159.

Hill, V.K., Kim, J.S., and Waldman, T. (2016). Cohesin mutations in human cancer. Biochimica et biophysica acta *1866*, 1-11.

Johmura, Y., Shimada, M., Misaki, T., Naiki-Ito, A., Miyoshi, H., Motoyama, N., Ohtani, N., Hara, E., Nakamura, M., Morita, A.*, et al.* (2014). Necessary and sufficient role for a mitosis skip in senescence induction. Molecular cell *55*, 73-84.

Krenning, L., Feringa, F.M., Shaltiel, I.A., van den Berg, J., and Medema, R.H. (2014). Transient activation of p53 in G2 phase is sufficient to induce senescence. Molecular cell *55*, 59-72.

Kueng, S., Hegemann, B., Peters, B.H., Lipp, J.J., Schleiffer, A., Mechtler, K., and Peters, J.M. (2006). Wapl controls the dynamic association of cohesin with chromatin. Cell *127*, 955-967.

Lamm, N., Ben-David, U., Golan-Lev, T., Storchova, Z., Benvenisty, N., and Kerem, B. (2016). Genomic Instability in Human Pluripotent Stem Cells Arises from Replicative Stress and Chromosome Condensation Defects. Cell stem cell *18*, 253-261.

Lukas, C., Savic, V., Bekker-Jensen, S., Doil, C., Neumann, B., Pedersen, R.S., Grofte, M., Chan, K.L., Hickson, I.D., Bartek, J.*, et al.* (2011). 53BP1 nuclear bodies form around DNA lesions generated by mitotic transmission of chromosomes under replication stress. Nature cell biology *13*, 243-253.

Martinez, P., Thanasoula, M., Munoz, P., Liao, C., Tejera, A., McNees, C., Flores, J.M., Fernandez-Capetillo, O., Tarsounas, M., and Blasco, M.A. (2009). Increased telomere fragility and fusions resulting from TRF1 deficiency lead to degenerative pathologies and increased cancer in mice. Genes & development *23*, 2060-2075.

Miller, K.M., Rog, O., and Cooper, J.P. (2006). Semi-conservative DNA replication through telomeres requires Taz1. Nature *440*, 824-828.

Minocherhomji, S., Ying, S., Bjerregaard, V.A., Bursomanno, S., Aleliunaite, A., Wu, W., Mankouri, H.W., Shen, H., Liu, Y., and Hickson, I.D. (2015). Replication stress activates DNA repair synthesis in mitosis. Nature *528*, 286-290.

Musacchio, A. (2015). The Molecular Biology of Spindle Assembly Checkpoint Signaling Dynamics. Curr Biol *25*, R1002-1018.

Rolef Ben-Shahar, T., Heeger, S., Lehane, C., East, P., Flynn, H., Skehel, M., and Uhlmann, F. (2008). Eco1-dependent cohesin acetylation during establishment of sister chromatid cohesion. Science (New York, N.Y *321*, 563-566.

Roos, W.P., Thomas, A.D., and Kaina, B. (2016). DNA damage and the balance between survival and death in cancer biology. Nature reviews *16*, 20-33.

Sakaue-Sawano, A., Kurokawa, H., Morimura, T., Hanyu, A., Hama, H., Osawa, H., Kashiwagi, S., Fukami, K., Miyata, T., Miyoshi, H.*, et al.* (2008). Visualizing spatiotemporal dynamics of multicellular cell-cycle progression. Cell *132*, 487-498.

Salic, A., Waters, J.C., and Mitchison, T.J. (2004). Vertebrate shugoshin links sister centromere cohesion and kinetochore microtubule stability in mitosis. Cell *118*, 567-578.

Sansregret, L., and Swanton, C. (2017). The Role of Aneuploidy in Cancer Evolution. Cold Spring Harb Perspect Med *7*.

Santaguida, S., Tighe, A., D'Alise, A.M., Taylor, S.S., and Musacchio, A. (2010). Dissecting the role of MPS1 in chromosome biorientation and the spindle checkpoint through the small molecule inhibitor reversine. The Journal of cell biology *190*, 73-87.

Sapkota, H., Wasiak, E., Daum, J.R., and Gorbsky, G.J. (2018). Multiple determinants and consequences of cohesion fatigue in mammalian cells. Molecular biology of the cell *29*, 1811-1824.

Sfeir, A., Kosiyatrakul, S.T., Hockemeyer, D., MacRae, S.L., Karlseder, J., Schildkraut, C.L., and de Lange, T. (2009). Mammalian telomeres resemble fragile sites and require TRF1 for efficient replication. Cell *138*, 90-103.

Sumara, I., Vorlaufer, E., Gieffers, C., Peters, B.H., and Peters, J.M. (2000). Characterization of vertebrate cohesin complexes and their regulation in prophase. The Journal of cell biology *151*, 749-762.

Tang, Z., Sun, Y., Harley, S.E., Zou, H., and Yu, H. (2004). Human Bub1 protects centromeric sister-chromatid cohesion through Shugoshin during mitosis. Proceedings of the National Academy of Sciences of the United States of America *101*, 18012-18017.

Tedeschi, A., Wutz, G., Huet, S., Jaritz, M., Wuensche, A., Schirghuber, E., Davidson, I.F., Tang, W., Cisneros, D.A., Bhaskara, V.*, et al.* (2013). Wapl is an essential regulator of chromatin structure and chromosome segregation. Nature *501*, 564-568.

Thompson, S.L., and Compton, D.A. (2010). Proliferation of aneuploid human cells is limited by a p53-dependent mechanism. The Journal of cell biology *188*, 369-381.

Tittel-Elmer, M., Lengronne, A., Davidson, M.B., Bacal, J., François, P., Hohl, M., Petrini, J.H.J., Pasero, P., and Cobb, J.A. (2012). Cohesin Association to Replication Sites Depends on Rad50 and Promotes Fork Restart. Molecular cell *48*, 98-108.

Van Ly, D., Low, R.R.J., Frolich, S., Bartolec, T.K., Kafer, G.R., Pickett, H.A., Gaus, K., and Cesare, A.J. (2018). Telomere Loop Dynamics in Chromosome End Protection. Molecular cell *71*, 510-525 e516.

Vitale, I., Galluzzi, L., Castedo, M., and Kroemer, G. (2011). Mitotic catastrophe: a mechanism for avoiding genomic instability. Nature reviews *12*, 385-392.

Wei, M.C., Zong, W.X., Cheng, E.H., Lindsten, T., Panoutsakopoulou, V., Ross, A.J., Roth, K.A., MacGregor, G.R., Thompson, C.B., and Korsmeyer, S.J. (2001). Proapoptotic BAX and BAK: a requisite gateway to mitochondrial dysfunction and death. Science (New York, N.Y *292*, 727-730.

Wutz, G., Várnai, C., Nagasaka, K., Cisneros, D.A., Stocsits, R.R., Tang, W., Schoenfelder, S., Jessberger, G., Muhar, M., Hossain, M.J.*, et al.* (2017). Topologically associating domains and chromatin loops depend on cohesin and are regulated by CTCF, WAPL, and PDS5 proteins. The EMBO journal *36*, e201798004.

Zeman, M.K., and Cimprich, K.A. (2014). Causes and consequences of replication stress. Nature cell biology *16*, 2-9.

Zhang, J., Shi, X., Li, Y., Kim, B.J., Jia, J., Huang, Z., Yang, T., Fu, X., Jung, S.Y., Wang, Y.*, et al.* (2008). Acetylation of Smc3 by Eco1 is required for S phase sister chromatid cohesion in both human and yeast. Molecular cell *31*, 143-151.

Figure 1

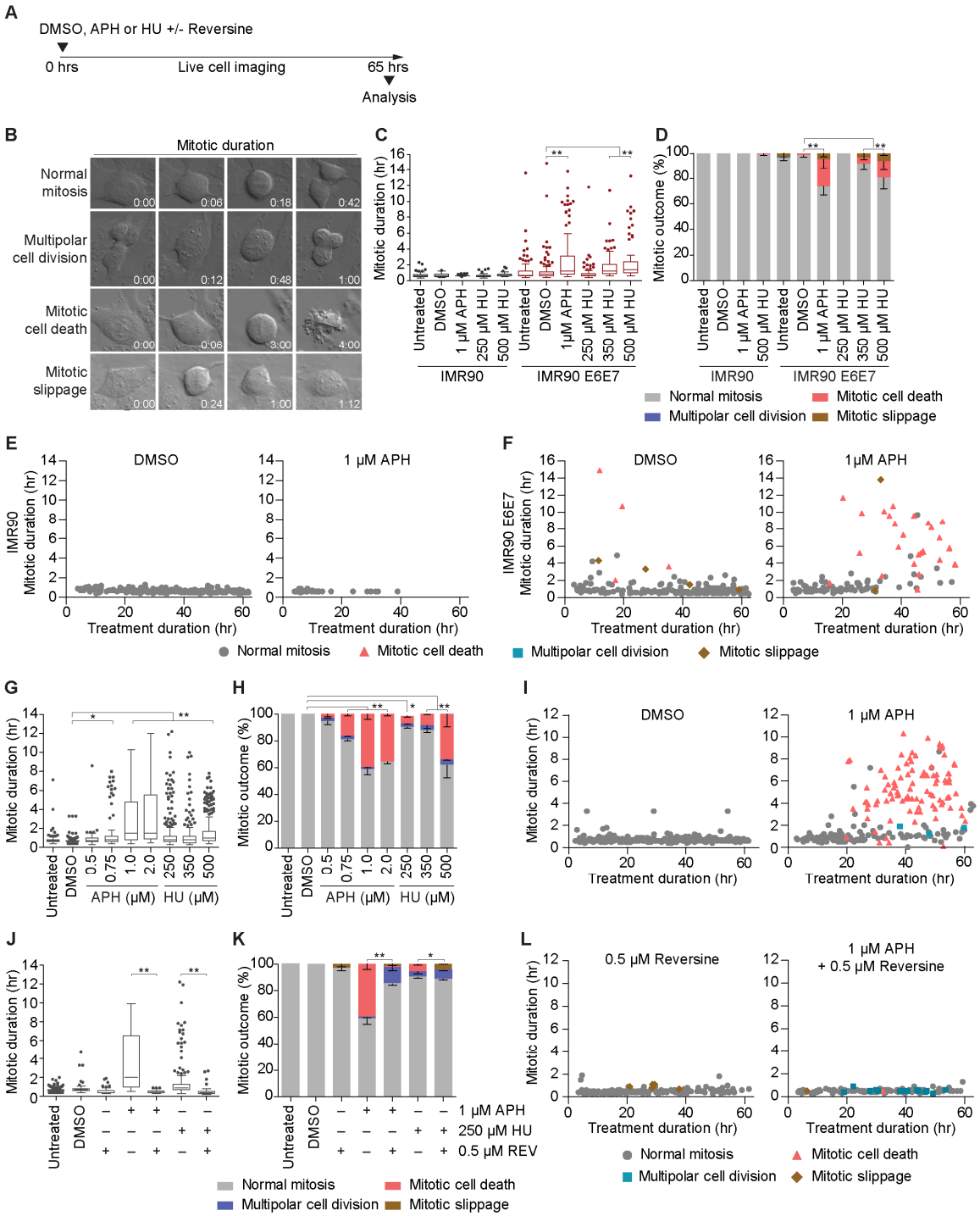
A
DMSO, APH or HU +/- Reversine
0 hrs
Live cell imaging
65 hrs
Analysis
B
Mitotic duration
Normal mitosis
Multipolar cell division
Mitotic cell death
Mitotic slippage
C
Mitotic duration (hr)
Untreated
DMSO
1 μM APH
250 μM HU
500 μM HU
350 μM HU
IMR90
IMR90 E6E7
D
Mitotic outcome (%)
Normal mitosis
Mitotic cell death
Multipolar cell division
Mitotic slippage
E
DMSO
1 μM APH
IMR90 Mitotic duration (hr)
Treatment duration (hr)
F
IMR90 E6E7 Mitotic duration (hr)
G
H
APH (μM)
HU (μM)
I
J
K
1 μM APH
250 μM HU
0.5 μM REV
L
0.5 μM Reversine
1 μM APH
+ 0.5 μM Reversine

Figure 1: Replication stress induces SAC-dependent mitotic arrest and mitotic death. A) Time course of live cell imaging throughout this study unless indicated otherwise. B) Representative images depicting mitotic outcome and duration from DIC live cell imaging experiments. Time is shown as (hr:min) relative to the first image of the series. C) Mitotic duration of IMR90 or IMR90 E6E7 cells following treatment with DMSO, APH or HU (three biological replicates scoring n ≥ 46 mitoses per condition for IMR90 or n ≥ 66 mitoses per condition for IMR90 E6E7 are compiled in a Tukey box plot, Mann-Whitney test). D) Outcome of the mitotic events in (C) (mean ± s.e.m, n = 3 biological replicates, Fisher's Exact Test). E and F) Two-dimensional dot plots for IMR90 (E) and IMR90 E6E7 (F) of mitotic duration and outcome for the data shown in (C, D). Each symbol represents an individual mitosis. T = 0 hr is when DMSO or APH were added to the culture. Location of a symbol on the x-axis indicates the time after treatment when that mitosis initiated, the height on the y-axis represents mitotic duration, and the symbol corresponds to mitotic outcome. G) Mitotic duration of HT1080 6TG cells following treatment with DMSO, APH, or HU (three biological replicates scoring n ≥ 92 mitotic events per condition compiled in a Tukey box plot, Mann-Whitney test). H) Outcome of the mitotic events in (G) (mean ± s.e.m, n = 3 biological replicates, Fisher's Exact Test). I) Two-dimensional dot plots of mitotic duration and outcome from (G, H). J) Mitotic duration of HT1080 6TG cultures treated with DMSO, APH or HU ± Reversine (REV) (three biological replicates scoring ≥ 112 mitotic events per each condition compiled in a Tukey box plot, Mann-Whitney test). K) Outcome of mitotic events in (J) (mean ± s.e.m, n = 3 biological replicates, Fisher's Exact Test). L) Two-dimensional plots of mitotic duration and outcome from (J, K). For all panels, * $p < 0.05$, ** $p < 0.01$.

Figure 2

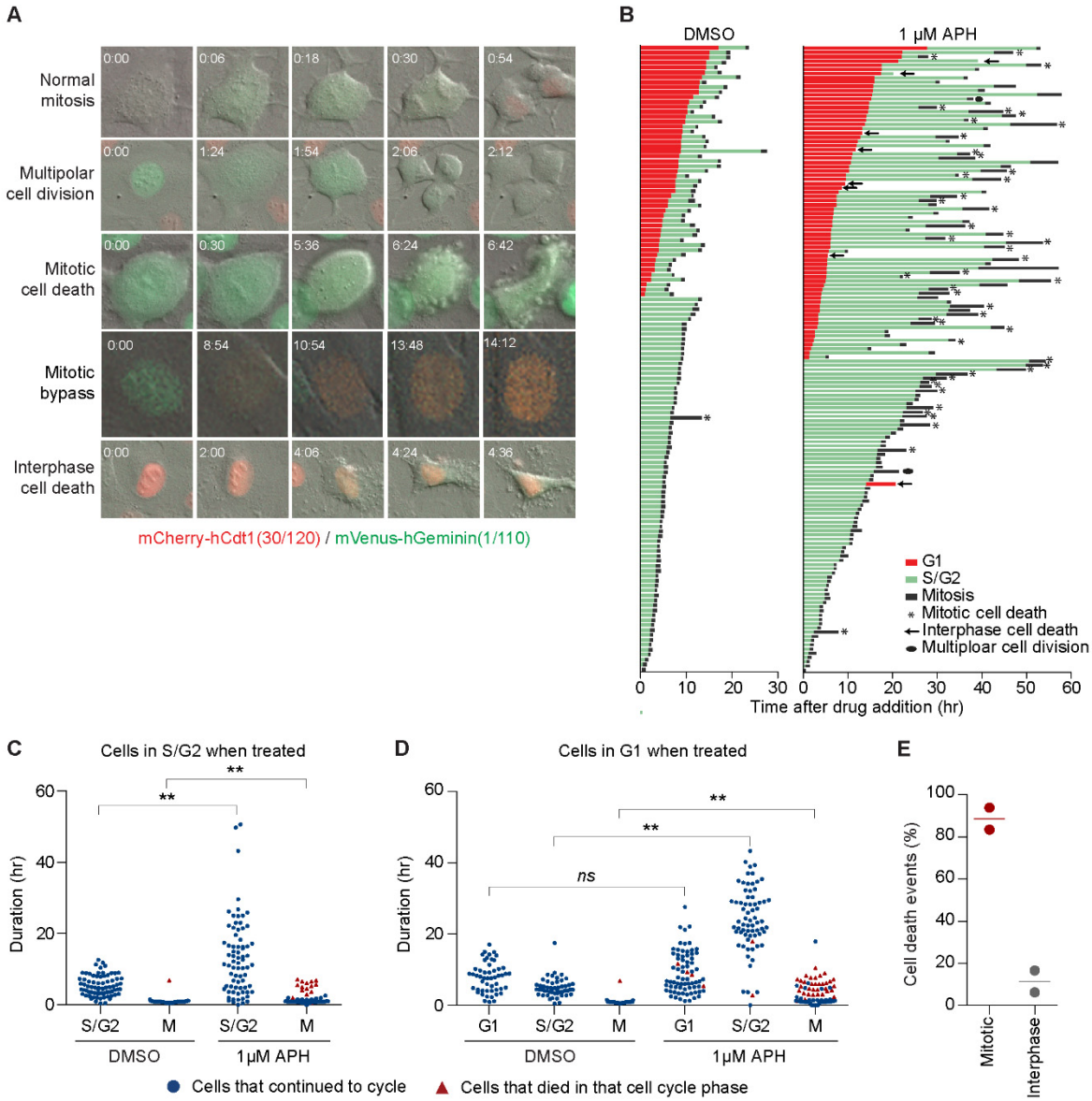
A
Normal mitosis
Multipolar cell division
Mitotic cell death
Mitotic bypass
Interphase cell death
mCherry-hCdt1(30/120) / mVenus-hGeminin(1/110)
B
DMSO
1 μM APH
G1
S/G2
Mitosis
Mitotic cell death
Interphase cell death
Multiploar cell division
Time after drug addition (hr)
C
Cells in S/G2 when treated
Duration (hr)
S/G2
M
DMSO
1μM APH
D
Cells in G1 when treated
ns
G1
E
Cell death events (%)
Mitotic
Interphase
Cells that continued to cycle
Cells that died in that cell cycle phase

Figure 2: Replication stress induces mitotic death in the same cell cycle. A) Representative images from live cell microscopy of HT1080 6TG-FUCCI cells. Time is shown as (hr:min) relative to the first image of the series. B) Cell fate map of HT1080 6TG-FUCCI live cell imaging. Each bar represents an individual cell as it progresses through the first imaged cell cycle to mitosis, or cell death, relative to addition of DMSO (n =127) or APH (n = 148) at T=0. Segment length represents the duration a cell spent in each cell cycle phase. Cell cycle phase are color coded according to FUCCI and shown in the legend. Data are from two independent biological replicates compiled into a single graph. C and D) Cell cycle phase duration and outcome for HT1080 6TG-FUCCI live cell imaging shown in (B). Data are sorted based on cells that were in S/G2 at the time DMSO or APH as administered (C), and cells that were in G1 at the time the DMSO or APH was administered (D). Symbols indicate if a cell survived that cell cycle phase and progressed, or if the cell died during that cell cycle phase. Data are from two independent biological replicates, compiled into a dot plot (Mann-Whitney test, ** $p < 0.01$). E) Categorization of all cell death events from (B) in HT1080 6TG-FUCCI cells in the first cell cycle with APH treatment.

Figure 3

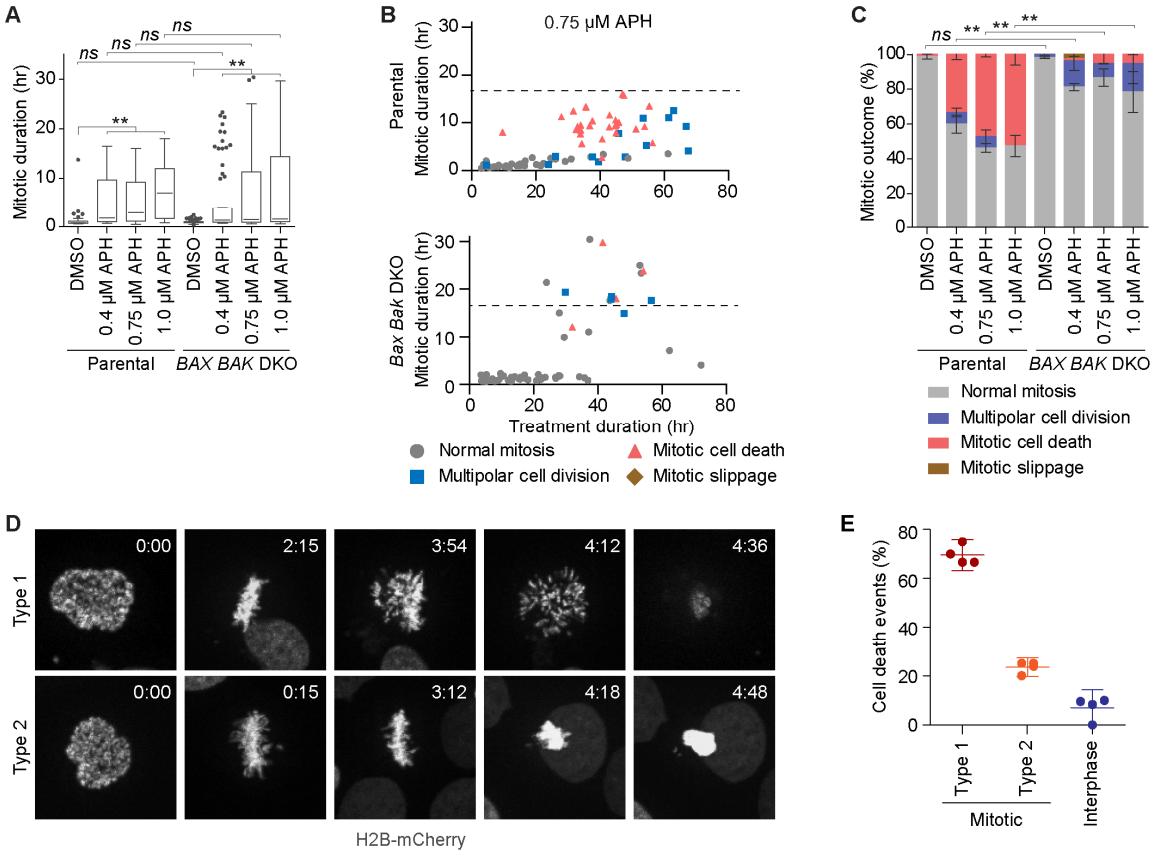
A
Mitotic duration (hr)
ns
ns
ns
ns
**
**
DMSO
0.4 μM APH
0.75 μM APH
1.0 μM APH
Parental
BAX BAK DKO
B
0.75 μM APH
Parental Mitotic duration (hr)
Bax Bak DKO Mitotic duration (hr)
Treatment duration (hr)
Normal mitosis
Multipolar cell division
Mitotic cell death
Mitotic slippage
C
Mitotic outcome (%)
ns
**
**
**
Normal mitosis
Multipolar cell division
Mitotic cell death
Mitotic slippage
D
Type 1
Type 2
0:00
2:15
3:54
4:12
4:36
0:00
0:15
3:12
4:18
4:48
H2B-mCherry
E
Cell death events (%)
Type 1
Type 2
Interphase
Mitotic

Figure 3: Replication stress induces distinct types of mitotic death. A) Mitotic duration of HeLa parental and *BAX BAK* DKO cells following treatment with DMSO or APH (three biological replicates using independent clones scoring n ≥ 32 mitotic events per condition are compiled in a Tukey box plot, Mann-Whitney test). B) Two-dimensional dot plots of mitotic duration and outcome in 0.75 μM APH treated HeLa parental and *BAX BAK* DKO cells from (A). The dashed line identifies the longest duration mitosis observed in the parental cells. C) Outcome of the mitotic events in (A)(mean ± s.e.m, n = 3 biological replicates using independent clones, Fisher's Exact Test, ** $p < 0.01$, *ns* = not significant). D) Representative images of Type 1 and Type 2 mitotic death in 1 μM APH treated HT1080 6TG H2B-mCherry cells. Time is shown as (hr:min) relative to the first image of the series. E) Quantitation of cell death events in 1 μM APH treated HT1080 6TG H2B-mCherry cultures (mean ± s.d., n = 4 biological replicates scoring ≥ 91 mitotic events per condition).

Figure 4

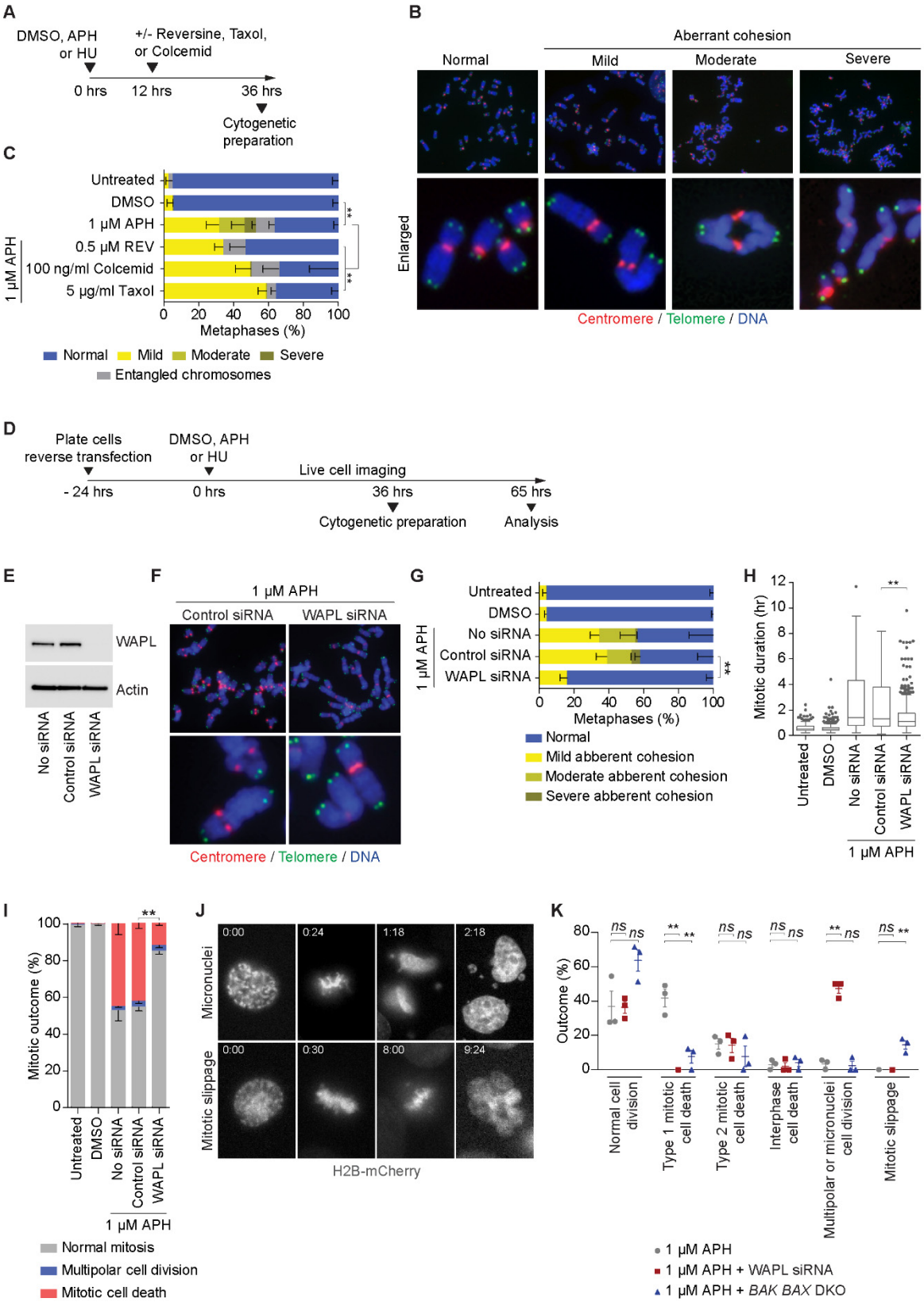
A
DMSO, APH or HU
+/- Reversine, Taxol, or Colcemid
0 hrs
12 hrs
36 hrs
Cytogenetic preparation
B
Aberrant cohesion
Normal
Mild
Moderate
Severe
Enlarged
Centromere / Telomere / DNA
C
Untreated
DMSO
1 μM APH
0.5 μM REV
100 ng/ml Colcemid
5 μg/ml Taxol
1 μM APH
Metaphases (%)
Normal
Mild
Moderate
Severe
Entangled chromosomes
D
Plate cells reverse transfection
DMSO, APH or HU
Live cell imaging
- 24 hrs
0 hrs
36 hrs
65 hrs
Cytogenetic preparation
Analysis
E
WAPL
Actin
No siRNA
Control siRNA
WAPL siRNA
F
1 μM APH
Control siRNA
WAPL siRNA
Centromere / Telomere / DNA
G
Untreated
DMSO
No siRNA
Control siRNA
WAPL siRNA
1 μM APH
Metaphases (%)
Normal
Mild abberent cohesion
Moderate abberent cohesion
Severe abberent cohesion
H
Mitotic duration (hr)
Untreated
DMSO
No siRNA
Control siRNA
WAPL siRNA
1 μM APH
I
Mitotic outcome (%)
Untreated
DMSO
No siRNA
Control siRNA
WAPL siRNA
1 μM APH
Normal mitosis
Multipolar cell division
Mitotic cell death
J
Micronuclei
Mitotic slippage
H2B-mCherry
K
Outcome (%)
Normal cell division
Type 1 mitotic cell death
Type 2 mitotic cell death
Interphase cell death
Multipolar or micronuclei cell division
Mitotic slippage
1 μM APH
1 μM APH + WAPL siRNA
1 μM APH + BAK BAX DKO

Figure 4: WAPL drives cohesion fatigue and *BAX*/*BAK*-dependent Type 1 mitotic death. A) Time course for experimentation in (B, C). B) Representative images of cytogenetic chromosome spreads from HT1080 6TG cells stained with DAPI (blue), centromere PNA (red) and telomere PNA (green) depicting the replication stress-induced cohesion phenotypes. C) Quantitation of cohesion phenotypes depicted in (B) in HT1080 6TG cells treated with DMSO or APH, ± Reversine (REV), Colcemid or Taxol (mean ± s.e.m, n= 3 biological replicates scoring ≥ 152 chromosome spreads per condition, Fisher's Exact Test). D) Experimental time course for (E-K). E) Western blots of whole cell extracts from HT1080 6TG cells treated with WAPL or control siRNA. F) Representative images of cytogenetic chromosome spreads from HT1080 6TG cells treated with APH and siRNA. G) Quantitation of cohesion phenotypes in HT1080 6TG cells treated with APH ± siRNA (mean ± s.e.m, n= 3 biological replicates scoring ≥ 144 chromosome spreads per condition, Fisher's Exact Test). H) Mitotic duration of HT1080 6TG cells treated with APH ± siRNA (three biological replicates scoring n ≥ 429 mitoses per condition are compiled in a Tukey box plot, Mann-Whitney test). I) Outcome of the mitotic events in (H) (mean ± s.e.m, n = 3 biological replicates, Fisher's Exact Test). J) Representative images of cell division generating micronuclei, or mitotic slippage, in APH treated HT1080 6TG H2B-mCherry cells. K) Mitotic outcomes in HT1080 6TG H2B-mCherry cells treated with APH ± WAPL siRNA or *BAX BAK* DKO (n = 97 APH, n = 38 APH + WAPL knock down, n = 88 APH + *BAX BAK* DKO cells, Student t-test or Fisher's Exact test). For all panels, *ns* = not significant, ** $p < 0.01$.

Figure 5

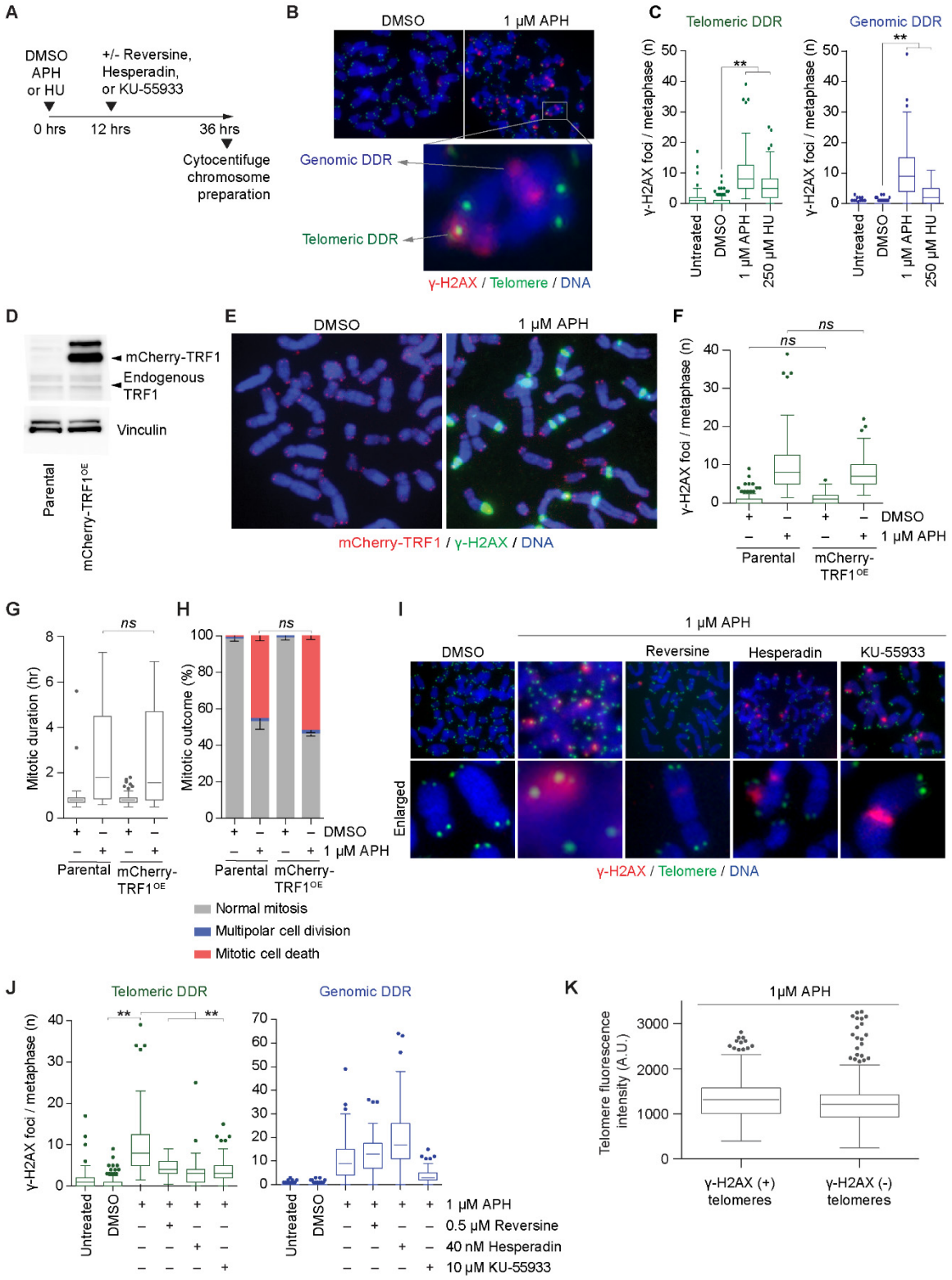
A
DMSO
APH
or HU
+/- Reversine,
Hesperadin,
or KU-55933
0 hrs
12 hrs
36 hrs
Cytocentifuge
chromosome
preparation
B
DMSO
1 μM APH
Genomic DDR
Telomeric DDR
γ-H2AX / Telomere / DNA
C
Telomeric DDR
Genomic DDR
γ-H2AX foci / metaphase (n)
Untreated
DMSO
1 μM APH
250 μM HU
D
mCherry-TRF1
Endogenous TRF1
Vinculin
Parental
mCherry-TRF1OE
E
DMSO
1 μM APH
mCherry-TRF1 / γ-H2AX / DNA
F
ns
γ-H2AX foci / metaphase (n)
DMSO
1 μM APH
Parental
mCherry-TRF1OE
G
Mitotic duration (hr)
ns
Parental
mCherry-TRF1OE
H
Mitotic outcome (%)
ns
DMSO
1 μM APH
Parental
mCherry-TRF1OE
Normal mitosis
Multipolar cell division
Mitotic cell death
I
1 μM APH
DMSO
Reversine
Hesperadin
KU-55933
Enlarged
γ-H2AX / Telomere / DNA
J
Telomeric DDR
Genomic DDR
γ-H2AX foci / metaphase (n)
**
Untreated
DMSO
1 μM APH
0.5 μM Reversine
40 nM Hesperadin
10 μM KU-55933
K
1μM APH
Telomere fluorescence intensity (A.U.)
γ-H2AX (+) telomeres
γ-H2AX (-) telomeres

Figure 5: Lethal replication stress induces non-canonical mitotic telomere deprotection. A) Experimental time course for (B, C) B) Example images of cytocentrifuged chromosome spreads stained with DAPI (blue), γ-H2AX immunofluorescence (red) and telomere PNA FISH (green) in HT1080 6TG cells treated with DMSO or APH. C) Quantitation of telomeric and genomic DDR foci in APH or HU treated HT1080 6TG cells (three biological replicates scoring n ≥ 81 chromosome spreads per condition are compiled in a Tukey box plot, Mann-Whitney test). D) Western blot of whole cell extracts from HT1080 6TG parental and HT1080 6TG mCherry-TRF1^{OE} cells. E) Representative images of cytocentrifuged chromosomes from HT1080 6TG mCherry-TRF1^{OE} cells treated with DMSO or APH, stained with DAPI (blue) and γ-H2AX IF (green). F) Quantitation of telomeric DDR foci in HT1080 6TG parental and HT1080 6TG mCherry-TRF1^{OE} cells (two biological replicates scoring n ≥ 48 chromosome spreads per condition are compiled in a Tukey box plot, Mann-Whitney test). G) Mitotic duration of HT1080 6TG parental and HT1080 6TG mCherry-TRF1^{OE} cells with DMSO or APH treatment (three biological replicates scoring n ≥ 57 mitoses per condition compiled in a Tukey box plot, Mann-Whitney test). H) Outcome of the mitotic events in (G) (mean ± s.e.m, n = 3 biological replicates, Fisher's Exact Test). I) Representative images of the mitotic DDR on cytocentrifuged chromosome as shown in (B) for HT1080 6TG cells treated with APH ± Reversine, Hesperadin or KU-55933. J) Quantitation of telomere and genomic DDR foci for the conditions shown in (I) (three biological replicates scoring n ≥ 37 chromosome spreads per condition are compiled in a Tukey box plot, Mann-Whitney test). K) Telomere PNA FISH signal intensity in arbitrary units (A.U.) from individual telomeres in APH treated HT1080 6TG cells, sorted by γ-H2AX status (three biological replicates scoring n ≥ 1529 telomeres per condition compiled into a Tukey box plot, Mann-Whitney test). For all panels, *ns* = not significant, ** $p < 0.01$.

Figure 6

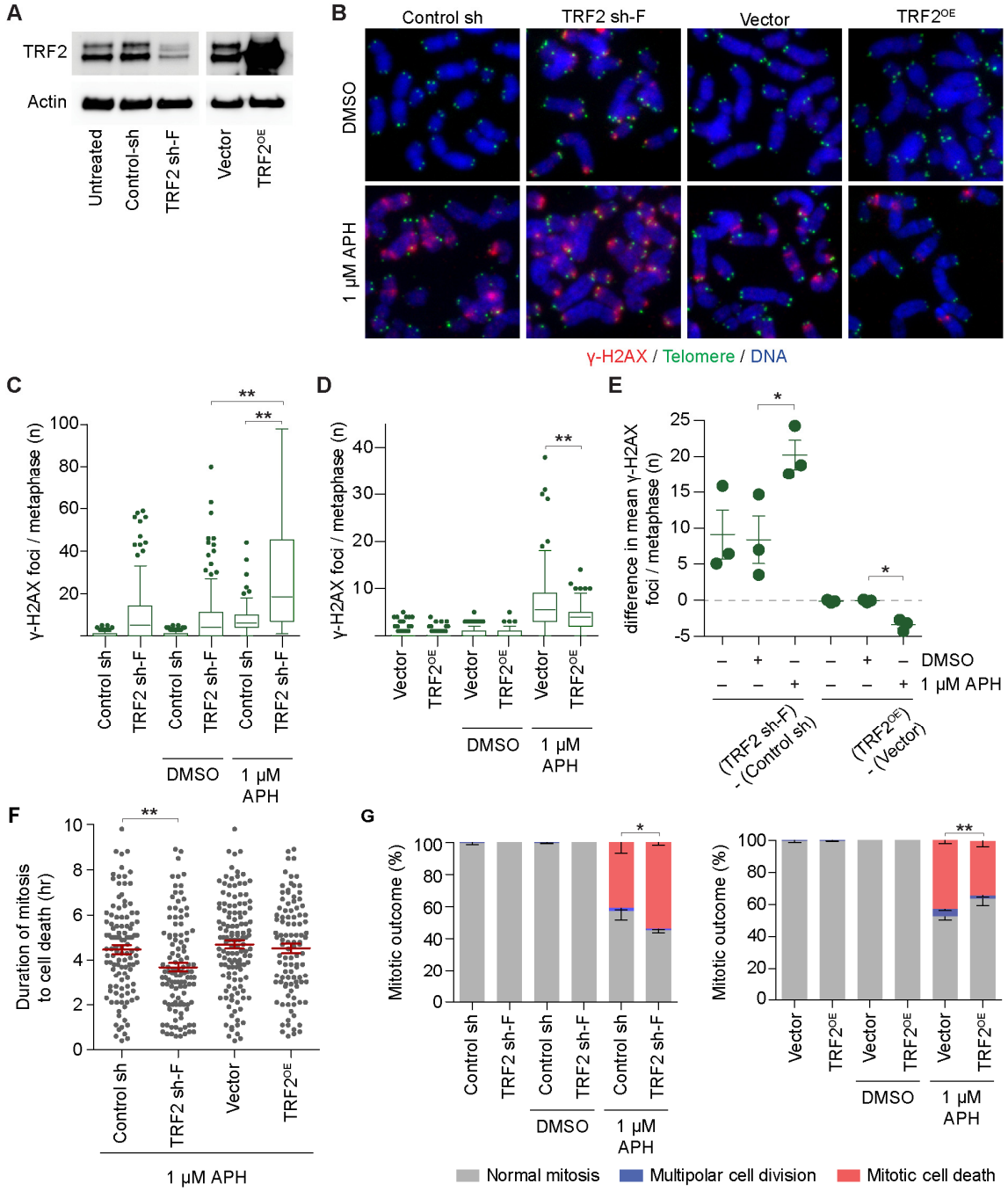
A
TRF2
Actin
Untreated
Control-sh
TRF2 sh-F
Vector
TRF2OE
B
Control sh
TRF2 sh-F
Vector
TRF2OE
DMSO
1 μM APH
γ-H2AX / Telomere / DNA
C
γ-H2AX foci / metaphase (n)
Control sh
TRF2 sh-F
DMSO
1 μM APH
D
γ-H2AX foci / metaphase (n)
Vector
TRF2OE
DMSO
1 μM APH
E
difference in mean γ-H2AX foci / metaphase (n)
DMSO
1 μM APH
(TRF2 sh-F) - (Control sh)
(TRF2OE) - (Vector)
F
Duration of mitosis to cell death (hr)
Control sh
TRF2 sh-F
Vector
TRF2OE
1 μM APH
G
Mitotic outcome (%)
Control sh
TRF2 sh-F
Vector
TRF2OE
DMSO
1 μM APH
Normal mitosis
Multipolar cell division
Mitotic cell death

Figure 6: Non-canonical telomere deprotection contributes to replication stress-induced lethality. A) Western blots of whole cell extracts from HT1080 6TG cells stably transduced with control, TRF2 shRNA (TRF sh-F) or TRF2 over expression ($TRF2^{OE}$) vectors. B) Representative images of cyto-centrifuged chromosome spreads stained with DAPI (blue), γ-H2AX IF (red) and telomere PNA (green) from control, TRF sh-F or $TRF2^{OE}$ HT1080 6TG cells treated with DMSO or APH. C and D) Quantitation of the telomere DDR foci from Control sh and TRF2 sh-F cells (C) or vector and $TRF2^{OE}$ cells (D) ± DMSO or APH (three biological replicates scoring n = 50 mitotic spreads per replicate compiled in a Tukey box plot, Mann-Whitney test). E) Difference in the mean number of telomeric γ-H2AX foci between HT1080 6TG TRF2 sh-F or $TRF2^{OE}$ cells and their appropriate vector control. These are a different representation of the same data shown in (C, D) (mean ± s.e.m, n = 3 three biological replications, Student's t-test). F) Mitotic duration to cell death in APH treated control, TRF2 sh-F and or $TRF2^{OE}$ cells (three biological replicates scoring ≥ 267 mitotic death events per condition are shown in a dot plot, mean ± s.e.m, Mann-Whitney test). G) Mitotic outcome of control, TRF2 sh-F and $TRF2^{OE}$ cells treated with APH or DMSO (mean ± s.e.m, n = 3 biological replicates of at least 267mitoses per condition, Fisher's Exact Test). For all panels, $*p < 0.05$, $**p < 0.01$.

Figure 7

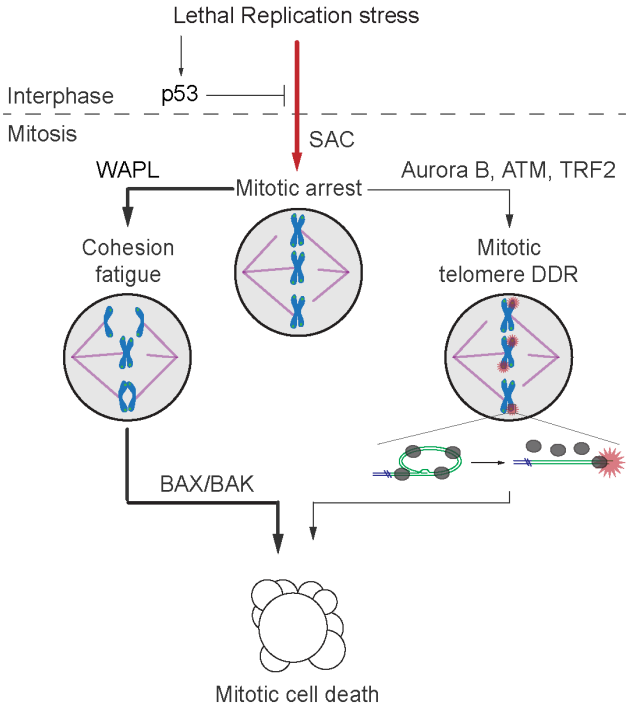

Figure 7: Model of replication stress-induced mitotic death. In p53-competent cells replication stress prevents mitotic entry, whereas lethal replication stress induces SAC-dependent mitotic arrest in cells lacking p53. Mitotic arrest then drives a dominant pathway of Type 1 cell death signalled via WAPL-dependent cohesion fatigue and BAX/BAK apoptosis. Non-canonical mitotic telomere deprotection contributes to a minority of mitotic lethality.

METHODS

Cell culture and treatments

HT1080 6TG cells were a kind gift from Eric Stanbridge (University of California, Irvine) and Saos-2 were provided by Roger Reddel (CMRI). IMR90 cells were purchased from ATCC and IMR90 E6E7 derived in the Karlseder laboratory. Phoenix cells were purchased from ATCC. Identity of all cell lines was verified by Cell Bank Australia using short tandem repeat profiling. HT1080 6TG, HeLa, Saos-2 and derivatives were cultured at 37º C, 10% CO_2, and atmospheric oxygen, in DMEM (Life Technologies) supplemented with 1% non-essential amino acids (Life Technologies), 1% Glutamax (Life Technologies), and 10% bovine growth serum (Hyclone). IMR90 and derivatives were cultured at 37º C, 10% CO_2, and 3% O_2, in DMEM, supplemented with 1% non-essential amino acids, 1% Glutamax, 10% fetal bovine serum (Life Technologies). The following compounds were used in cell treatments: dimethyl sulfoxide (DMSO, Sigma-Aldrich), Colcemid (Life Technologies), Taxol (Sigma), Reversine (Selleck Chemicals), KU-55933 (Calbiochem), Hesperadin (Selleck chemicals), Aphidicolin (Sigma-Aldrich) and Hydroxyurea (Sigma-Aldrich). All cell lines were tested for mycoplasma contamination (MycoAlert, LT07-118, Lonza) and were found to be negative.

Viral transduction and cell line generation

High titre, purified pLKO.1 derived lentiviral vectors, harbouring a non-targeting control shRNA (a gift from David Sabatini, addgene plasmid #1864), TRF2 sh-F (Open Biosystems, TRCN0000004811), or TRF2 sh-G (Open Biosystems, TRCN0000018358), were created by Leszek Lisowski in the Salk Institute Gene Transfer, Targeting and Therapeutics (GT3) core, or the CMRI Vector and Genome Engineering Facility as described elsewhere (Crabbe et al., 2012; Hayashi et al., 2012). Cell cultures were transduced with an MOI of 10 for 48 hours, then selected in normal growth media supplemented with 1 µg/ml Puromycin for five days. mVenus-hGeminin (1/110)/pCSII-EF and mCherry-hCdt1(30/120)/pCSII-EF (a kind gift from Atsushi Miyawaki) were individually packaged into lentivectors using 2nd generation packaging system, and the viral supernatants were used simultaneously to co-infect target cells. Three days post-transduction, cell cultures were sorted at the Salk Institute flow cytometry core for mVenus fluorescence, allowed to expand for 5 to 7 days, and sorted again for mCherry fluorescence. Proper progression of red/green coloration during cell cycling was confirmed with live cell imaging before use in experimentation. Retroviral vectors were created by transfecting Phoenix-AMPHO cells (purchased from ATCC) with pWZL-hygro (Vetctor, a gift from Scott Lowe, addgene plasmid #18750), pWZL Hygro-TRF2 (TRF2^{OE}, a gift from Titia

de Lange, addgene plasmid #16066), pWZL-hTERT (hTERT from pBabe-hTERT, a gift from Titia de Lange, was recloned into pWZL-hygro), pWZL-H2B-mCherry (Crabbe et al., 2012), pLPC-mCherry-TRF1 [mCherry was cloned into pLPC-NFLAG TRF1 (a gift from Titia de Lange, addgene plasmid #16058) by PCR amplification using BamHI restriction sites. Forward primer: 5'-CGG GGATCC ATG GTG AGC AAG GGC GAG GAGG-3' / Reverse primer: 5'-CGG GGATCC **GGT GGC GAT GCT GCG** CTT GTA CAG CTC GTC CAT GCC-3' A linker (bold) was added in C-terminus of mCherry], pLXSN3 or pLXSN3-p53DD (Hayashi et al 2015). Viral supernatants were used to infect HT1080 6TG or IMR90 cells. Stable vector and $TRF2^{OE}$ cell lines were selected by treatment with 100 µg/ml Hygromycin (Invitrogen). HT1080 6TG H2B-mCherry cells were sorted for mCherry fluorescence at the Salk Institute flow cytometry core facility. IMR90 TERT were selected with 100 µg/ml Hygromycin, followed by second infection with retrovirus carrying pLXSN3 or pLXSN3-p53DD and selection with 600 µg/ml G418 (Nacalai Tesque).

BAX BAK DKO cell line generation

HeLa, HT1080 6TG, and HT1080 6TG H2B-mCherry were transiently transfected with PX458 plasmids harbouring guide RNAs that target human BAX (5'-CTGCAGGATGATTGCCGCCG) or human BAK (5'-GCATGAAGTCGACCACGAAG) according to the manufacturer's protocol (XtremeGene; Sigma-Aldrich). Individual clones were initially screened for *BAX* and *BAK* deletion by immunoblotting, and then confirmed by sequencing.

siRNA transfection

Control non-targeting (control siRNA, D-001810-10) and WAPL (L-026287-01) ON-TARGETplus siRNA pools (Dharmacon) were transfected using Lipofectamine RNAi max (Thermofisher Scientific), according to the manufactures' protocols.

Live cell imaging and analysis

Differential interference contrast (DIC) microscopy was used to visualize mitotic duration and outcome. These experiments were performed on a ZEISS Cell Observer inverted wide field microscope, with 20x 0.8 NA air objective, at 37 ºC, 10% CO_2 and atmospheric oxygen. Images were captured every six minutes for a duration up to sixty-five hours using an Axiocam 506 monochromatic camera (ZEISS) and Zen software (ZEISS). FUCCI live cell imaging was

conducted on the same instrument, using the same imaging duration and protocol, with the addition of a ZEISS HXP 120C mercury short-arc lamp and compatible filter cubes, to obtain fluorescent images. Quantitative live cell imaging of mitotic chromosome dynamics in HT1080 6TG H2B-mCherry cultures and derivatives was done using either combined DIC and fluorescent imaging on the ZEISS Cell Observer described above with a 40x 0.95 NA plan-Apochromat air objective; or on a Zeiss Cell Observer SD spinning disk confocal microscope imaged using a 561nm, 50mW solid state excitation laser and appropriate filter sets with a 40x, 1.3 NA oil objective using an Evolve Delta camera (Photometrics). For these experiments, cells were cultured at 37º C, 10% CO_2 and atmospheric oxygen and images captured every three minutes for sixtry hours. For all movies, mitotic duration was scored by eye and calculated from nuclear envelope breakdown until cytokinesis or mitotic death. FUCCI Movies were scored by eye, for G1 (red) and S/G2 (green) by color, and for mitotic entry, duration and outcome by cell morphology. Chromosome dynamics in HT1080 6TG-mCherry H2B were scored by eye. All live cell imaging analysis was done using Zen software.

Visualization of chromatid cohesion and mitotic DDR activation

For cohesion analysis, standard methanol and acetic acid fixed cytogenetic chromosome spreads were prepared and stained with fluorescent in situ hybridization (FISH) with a telomere (Alexa488-OO-ccctaaccctaaccctaa), and centromere (Texas Red-OO-aaactagacagaagcatt), peptide nucleic acid (PNA) probes (Panagene), as described elsewhere (Cesare et al., 2015). The mitotic telomere DDR was visualized using the "metaphase-TIF assay" as described previously (Cesare et al., 2015). In this method, cells were cytocentrifuged onto glass slides, fixed and stained with telomere PNA FISH and immunofluorescence (IF) against γ-H2AX. For both assays, images were captured on a ZEISS AxioImager Z.2 with a 63x, 1.4 NA oil objective, appropriate filter cubes and a CoolCube1 camera (Metaystems). Automated metaphase finding and image acquisition for these experiments were done using the MetaSystems imaging platform as described elsewhere (Cesare et al., 2013).

Cytogenetic image analysis

Cytogenetic images were analysed using Isis software (MetaSystems). For cohesion analysis, images were scored by eye, and mitotic spreads classified as follows: normal, if < three chromosomes displayed visible separated sister chromatids; mild, if ≥ three chromosomes displayed visible sister chromatids; moderate if ≥ three chromosomes displayed centromere cohesion loss but retained distal chromosome arm cohesion; severe if ≥ three chromosomes

displayed complete sister chromatid separation. In practice, we typically observed the majority of chromosomes in a mitotic spread displayed the same cohesion status. Mitotic DDR foci were quantified by eye using Isis software, and classified as telomeric if the γ-H2AX IF focus colocalized with a telomere PNA signal. To determine relative telomere lengths at DDR (+) and DDR(-) chromosome ends, telomere signals were captured at fixed exposure time as described above, and images were analysed using Imaris software version 8.2 (BitPlane). Images were segmented using the mitotic chromosomes as a region of interest, and the telomeres were detected as spots using the spot detection wizard. Telomere colocalization with γ-H2AX foci were identified using the co-localisation tool. The sum fluorescence intensity was determined for each telomere in the γ-H2AX colocalised (DDR+) and the γ-H2AX excluded (DDR-) cohorts.

Chromatin fibre analysis

Replication rates were measured using chromatin fiber analysis as described elsewhere (Lamm et al., 2016). Briefly, unsynchronized cells are sequentially pulse-labelled with 100 μM of thymidine analogues (IdU then CldU) for 30 min each. After harvesting, the genomic DNA was stretched as fibres onto glass slides at a constant rate of 2 kb/μm using a molecular combing system (Genomic Vision). Nascent DNA replication was visualized by IF against IdU and CldU and captured using Zen software and a ZEISS AxioImager Z.2, with a 63x, 1.4 NA oil objective, appropriate filter cubes and an Axiocam 506 monochromatic camera (ZEISS). In our analysis, only replication forks with a visible origin of replication, and both IdU and CLdU staining were scored. Replication rates were calculated based solely on the IdU tracks, which result from the first pulse of nucleoside analogue. The length of IdU fibres were converted to kilobasepairs according to a constant and sequence-independent stretching factor (1 μm = 2 Kb) using Zen software.

Western blotting

Preparation of whole cell extracts and western blots were done as described elsewhere (Van Ly et al., 2018) and luminescence was visualized on an LAS 4000 Imager (Fujifilm).

Antibodies

Primary antibodies used in this study: γ-H2AX (05-636, Millipore), TRF2 (NB110-57130, Novus Biologicals), WAPL (SC-365189, Santa Cruz), β-actin (A5441, Sigma), BAX (rat monoclonal 49F9; WEHI monoclonal antibody facility), BAK (rabbit polyclonal B5897,

Sigma), CldU (6326, Abcam), and IdU (347580, BD Biosciences). Secondary antibodies used in this study: Alexa Fluor 568-Goat anti-mouse IgG (A-11031, Thermo Fisher Scientific), Alexa Fluor 488-Goat anti-mouse (A11029, Thermo Fisher Scientific) and Alexa Flour 594-Goat anti-rat IgG (A-11007). Goat anti-Rabbit HRP (P0448, Dako), Goat anti-Mouse HRP (P0447, Dako)

Statistics and Figure preparation

Statistical analysis was performed using GraphPad Prism. Box plots are displayed using the Tukey method where the box extends from the 25th to the 75th percentile data points and the line represents the median. The upper whisker represents data points ranging up to the 75th percentile + (1.5 × the inner quartile range), or the largest value data point if no data points are outside this range. The lower whisker represents data points ranging down to the 25th percentile – (1.5 × the inner quartile range), or the smallest data point if no data points are outside this range. Data points outside these ranges are shown as individual points. Error bars, statistical methods and n, are described in figure legends. In Fig. 4K statistical significance was determined by a t-test for all conditions expect mitotic slippage, where a Fisher's exact test was applied. This is because a t-test cannot be used when all outcomes are zero for two of the conditions. Figures were prepared using Adobe Photoshop and Illustrator.

SUPPLEMENTAL INFORMATION

Replication stress induces mitotic death through parallel pathways regulated by WAPL and telomere deprotection

V. Pragathi Masamsetti, Ka Sin Mak, Ronnie Ren Jie Low, Chris D. Riffkin, Noa Lamm, Laure Crabbe, Jan Karlseder, David C.S. Huang, Makoto T Hayashi & Anthony J. Cesare

Figures S1-S7
Movies S1-3

Figure S1

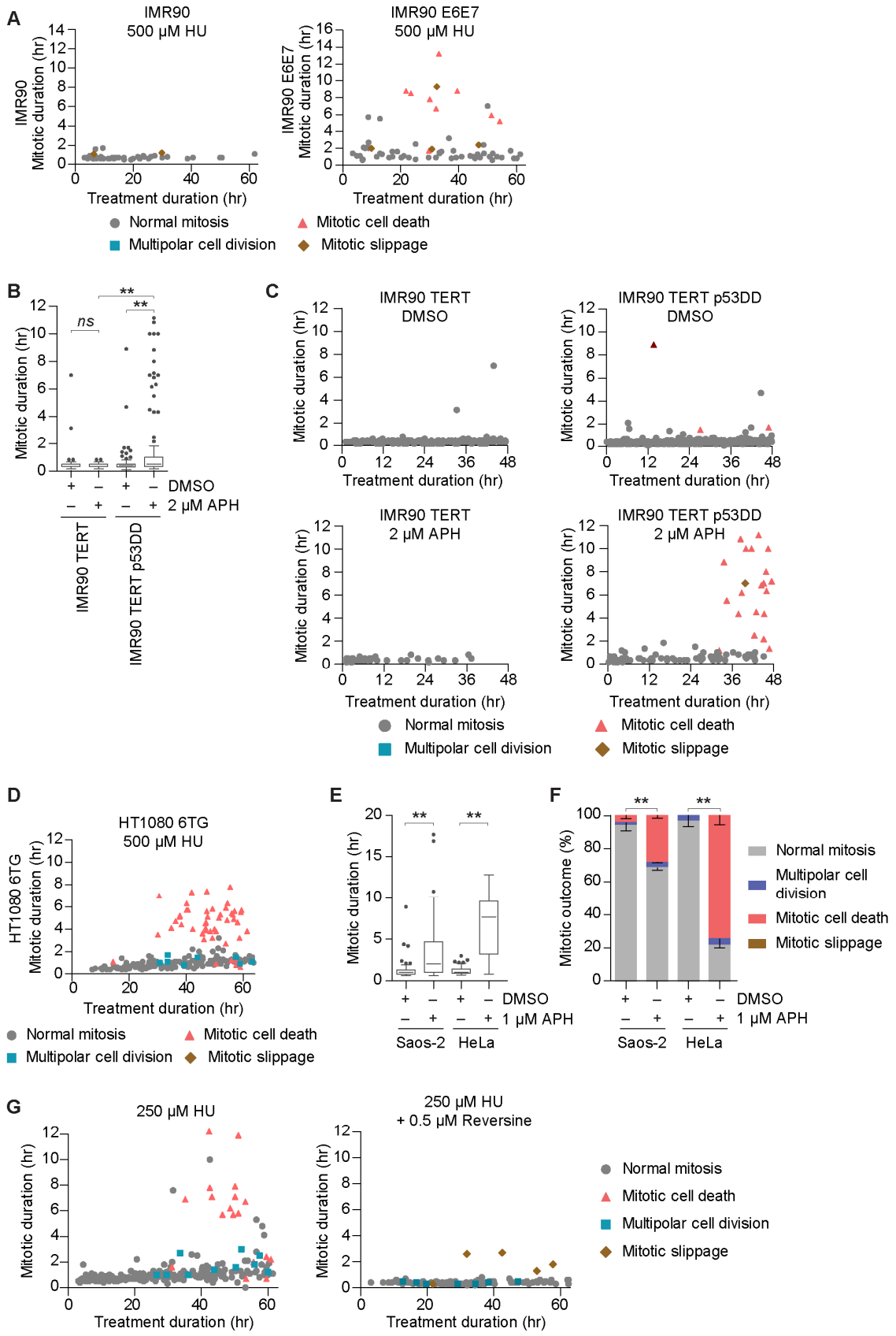
A
IMR90
500 μM HU
IMR90 Mitotic duration (hr)
Treatment duration (hr)
IMR90 E6E7
500 μM HU
IMR90 E6E7 Mitotic duration (hr)
Normal mitosis
Mitotic cell death
Multipolar cell division
Mitotic slippage
B
Mitotic duration (hr)
ns
**
**
DMSO
2 μM APH
IMR90 TERT
IMR90 TERT p53DD
C
IMR90 TERT
DMSO
IMR90 TERT p53DD
DMSO
IMR90 TERT
2 μM APH
IMR90 TERT p53DD
2 μM APH
Treatment duration (hr)
Normal mitosis
Mitotic cell death
Multipolar cell division
Mitotic slippage
D
HT1080 6TG
500 μM HU
HT1080 6TG Mitotic duration (hr)
Treatment duration (hr)
Normal mitosis
Mitotic cell death
Multipolar cell division
Mitotic slippage
E
Mitotic duration (hr)
DMSO
1 μM APH
Saos-2
HeLa
F
Mitotic outcome (%)
Normal mitosis
Multipolar cell division
Mitotic cell death
Mitotic slippage
DMSO
1 μM APH
Saos-2
HeLa
G
250 μM HU
Mitotic duration (hr)
Treatment duration (hr)
250 μM HU
+ 0.5 μM Reversine
Normal mitosis
Mitotic cell death
Multipolar cell division
Mitotic slippage

Figure S1. Lethal replication stress induces mitotic lethality in p53 compromised cells, related to Figure 1. A) Two-dimensional plots of mitotic duration and outcome from IMR90 and IMR90 E6E7 treated with Hydroxyurea (HU)(data corresponding to Fig. 1C, D). Data are presented as described in Fig. 1D (n = 46 mitoses for IMR90 and 66 mitoses for IMR90 E6E7 compiled from three biological replicates into a single graph). B) Mitotic duration of IMR90-TERT and IMR90-TERT p53DD treated with DMSO or Aphidicolin (APH) (Representative replicate showing ≥ 43 mitoses per condition compiled in a Tukey box plot, Mann-Whitney test). C) Two-dimensional plots of the data shown in (B). D) Two-dimensional plot of HT1080 6TG cells treated with 500 μM HU (data corresponding to Fig. 1G, H; n ≥ 200 mitoses compiled from three biological replicates into a single graph). E) Mitotic duration of Saos-2 and HeLa cells treated with DMSO or APH (three biological replicates scoring ≥ 43 mitoses per condition compiled in a Tukey box plot, Mann-Whitney test, *p < 0.01.) F) Outcome of the mitotic events in (E) (mean ± s.e.m, n = 3 biological replicates, Fisher's Exact Test). G), Two-dimensional plots of HT1080 6TG cells treated with Reversine ± HU (data corresponding to Fig. 1J, K; three biological replicates scoring n ≥ 112 mitoses per condition compiled into a single graph).

Figure S2

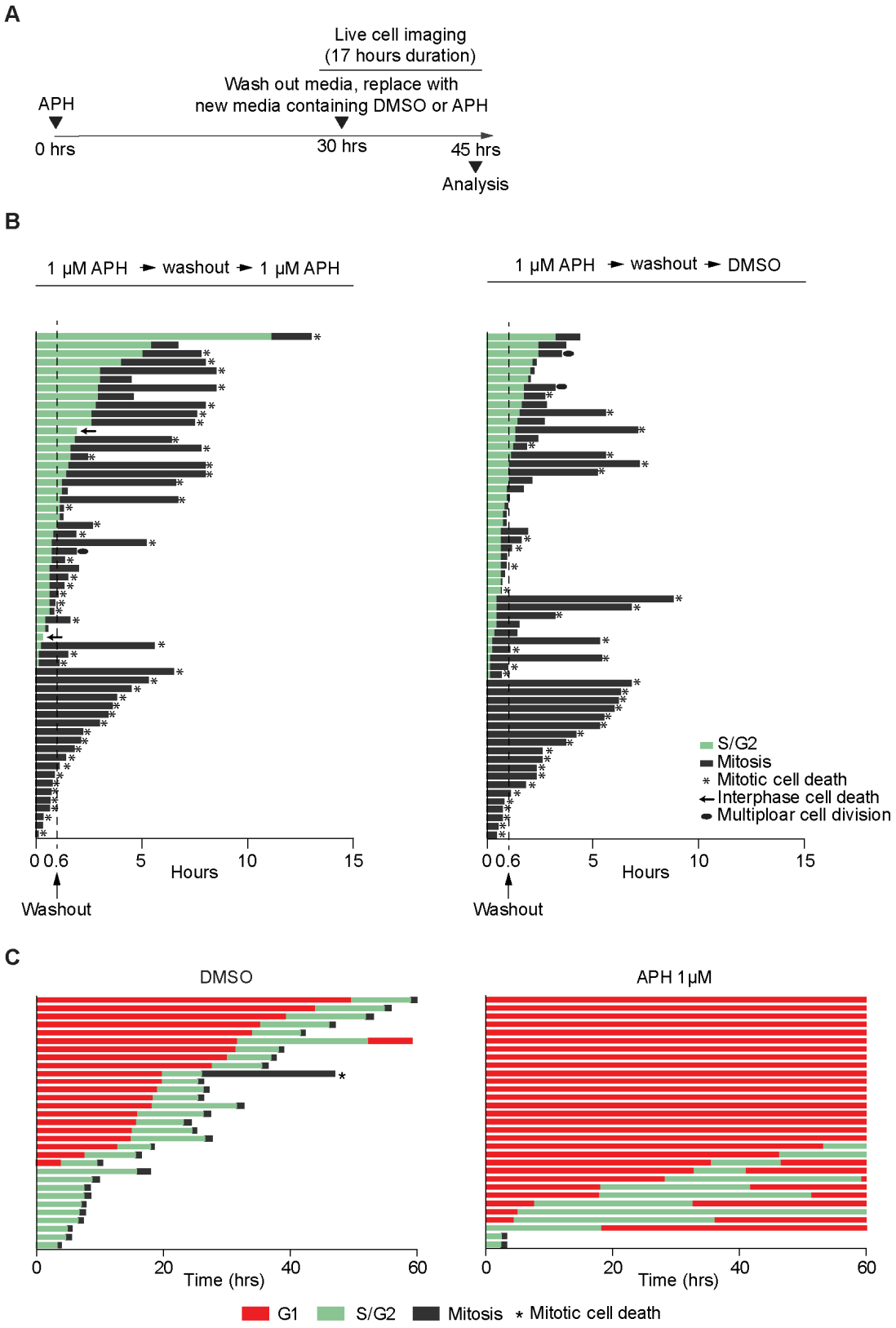
A
Live cell imaging
(17 hours duration)
Wash out media, replace with
new media containing DMSO or APH
APH
0 hrs
30 hrs
45 hrs
Analysis
B
1 μM APH → washout → 1 μM APH
1 μM APH → washout → DMSO
0 0.6 5 10 15
Hours
Washout
S/G2
Mitosis
Mitotic cell death
Interphase cell death
Multiploar cell division
C
DMSO
APH 1μM
0 20 40 60
Time (hrs)
G1
S/G2
Mitosis
Mitotic cell death

Figure S2. Mitotic arrest and death in p53-compromised cells occurs independent of mitotic APH treatment, and replication stress in p53-competent fibroblasts induces mitotic bypass, related to Figure 2. A) Timeline of experimentation in (B). B) Cell fate map of APH washout experiment in HT1080 6TG FUCCI cells. Cells were treated with APH for 30 hours, before media washout and replacement with fresh media containing APH or DMSO. The dotted line shows when the media was washed out and replaced. Each bar represents an individual cell as it progresses through cell division or death. Segment length represents the duration the cell spent in each cell cycle phase, which are color coded according to the legend. Data are from 2 independent biological replicates compiled into a single graph (n = 58 mitoses for each condition). C) Fate map of IMR90-FUCCI cells treated with DMSO or APH. Each bar represents an individual cell as it progresses through the first cell division, mitotic bypass, or cell death, relative to DMSO or APH treatment (T=0). Segment length represents the duration a cell spent in that cell cycle phase. One of three independent biological replicates are shown (n = 31 cells for each condition)

Figure S3

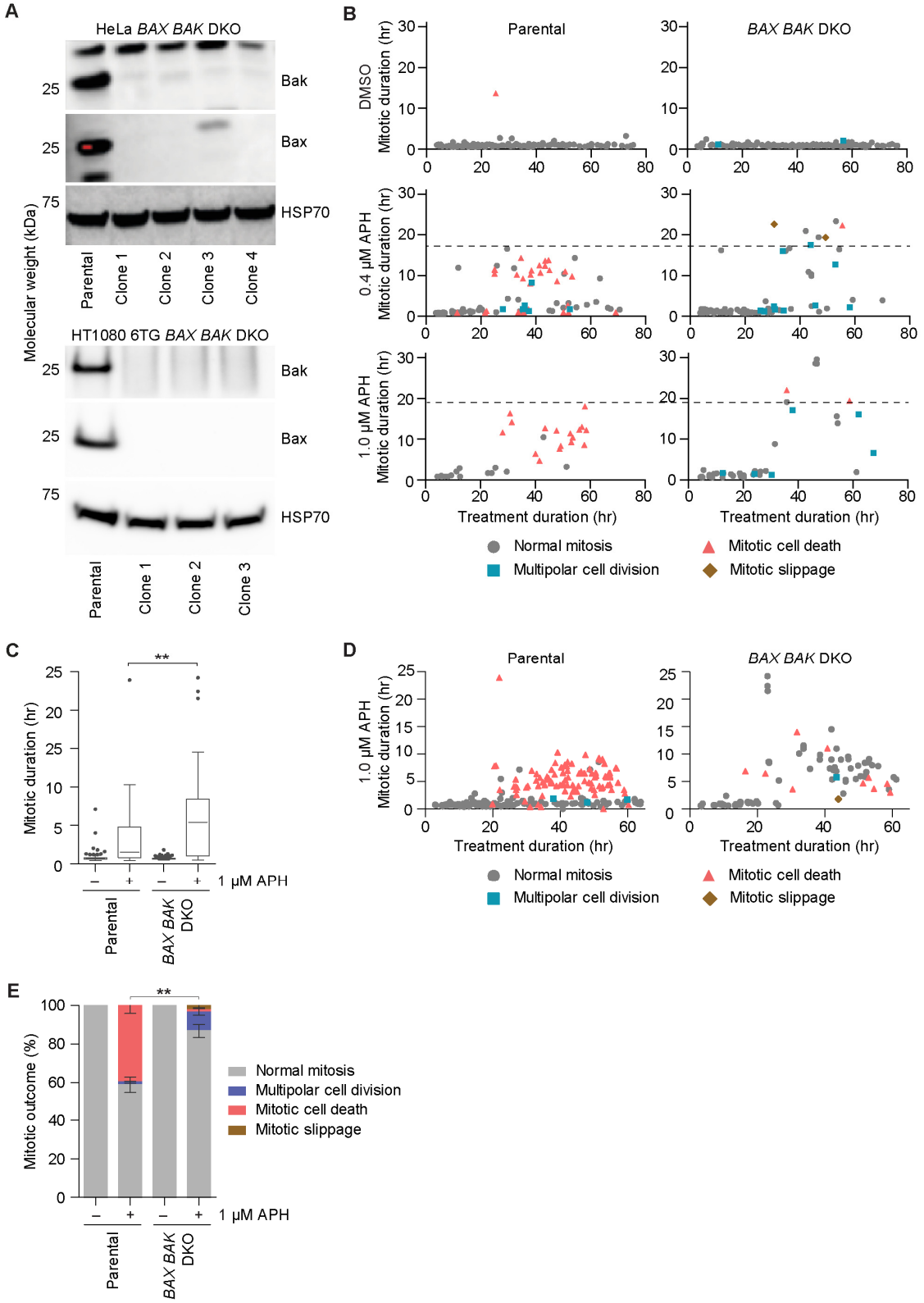
A
HeLa BAX BAK DKO
Bak
Bax
HSP70
Molecular weight (kDa)
25
25
75
Parental
Clone 1
Clone 2
Clone 3
Clone 4
HT1080 6TG BAX BAK DKO
Bak
Bax
HSP70
25
25
75
Parental
Clone 1
Clone 2
Clone 3
B
Parental
BAX BAK DKO
DMSO
0.4 μM APH
1.0 μM APH
Mitotic duration (hr)
Treatment duration (hr)
Normal mitosis
Multipolar cell division
Mitotic cell death
Mitotic slippage
C
Mitotic duration (hr)
**
1 μM APH
Parental
BAX BAK DKO
D
Parental
BAX BAK DKO
1.0 μM APH
Mitotic duration (hr)
Treatment duration (hr)
Normal mitosis
Multipolar cell division
Mitotic cell death
Mitotic slippage
E
Mitotic outcome (%)
**
Normal mitosis
Multipolar cell division
Mitotic cell death
Mitotic slippage
1 μM APH
Parental
BAX BAK DKO

Figure S3. Replication stress-induced mitotic death is primarily BAX/BAK-dependent, related to Figure 3. A) Western blots of whole cell extracts from HeLa (upper panels) and HT1080 6TG (lower panels) parental and *BAX BAK* DKO clones. B) Two-dimensional graphs of mitotic duration and outcome from HeLa parental and *BAX BAK* DKO cells shown in Fig 3A, B ($n \geq 32$ mitoses compiled from three biological replicates of independent DKO clones compiled into a single graph). The dashed line represents the longest mitotic event observed in the corresponding parental cells treated with the indicated dose of APH. C) Mitotic duration of HT1080 6TG parental and *BAX BAK* DKO cells treated with DMSO or APH (three biological replicates on independent DKO clones scoring ≥ 91 mitoses per condition are compiled into a Tukey box plot, Mann-Whitney test). D) Two-dimensional representation of mitotic duration and outcome of the data in (C and E). E) Mitotic outcome of the cells from (C and D, $n = 3$ biological replicates Fisher's exact test). For all panels ** $p < 0.01$.

Figure S4

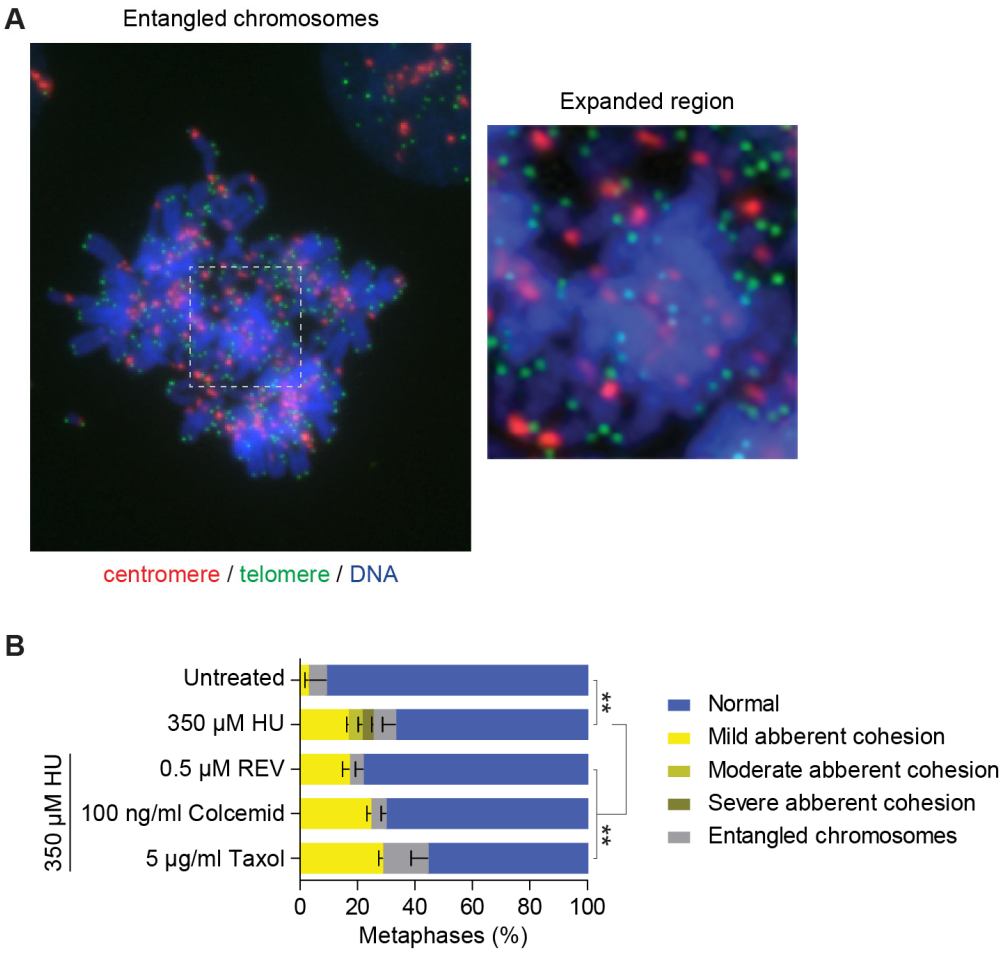

Figure S4. Lethal replication stress-induces entangles chromosomes and cohesion fatigue, related to Figure 4. A) Example image of entangled chromosomes, stained with DAPI (blue), and PNA FISH against the centromeres (red) and telomeres (green). B) Quantitation of cohesion phenotypes depicted in Fig. 4B in HT1080 6TG cells treated with DMSO or HU ± Reversine (REV), Colcemid or Taxol (mean ± s.e.m, n = 3 biological replicates scoring ≥ 70 chromosome spreads per condition, Fisher's Exact Test, **$p < 0.01$.).

Figure S5

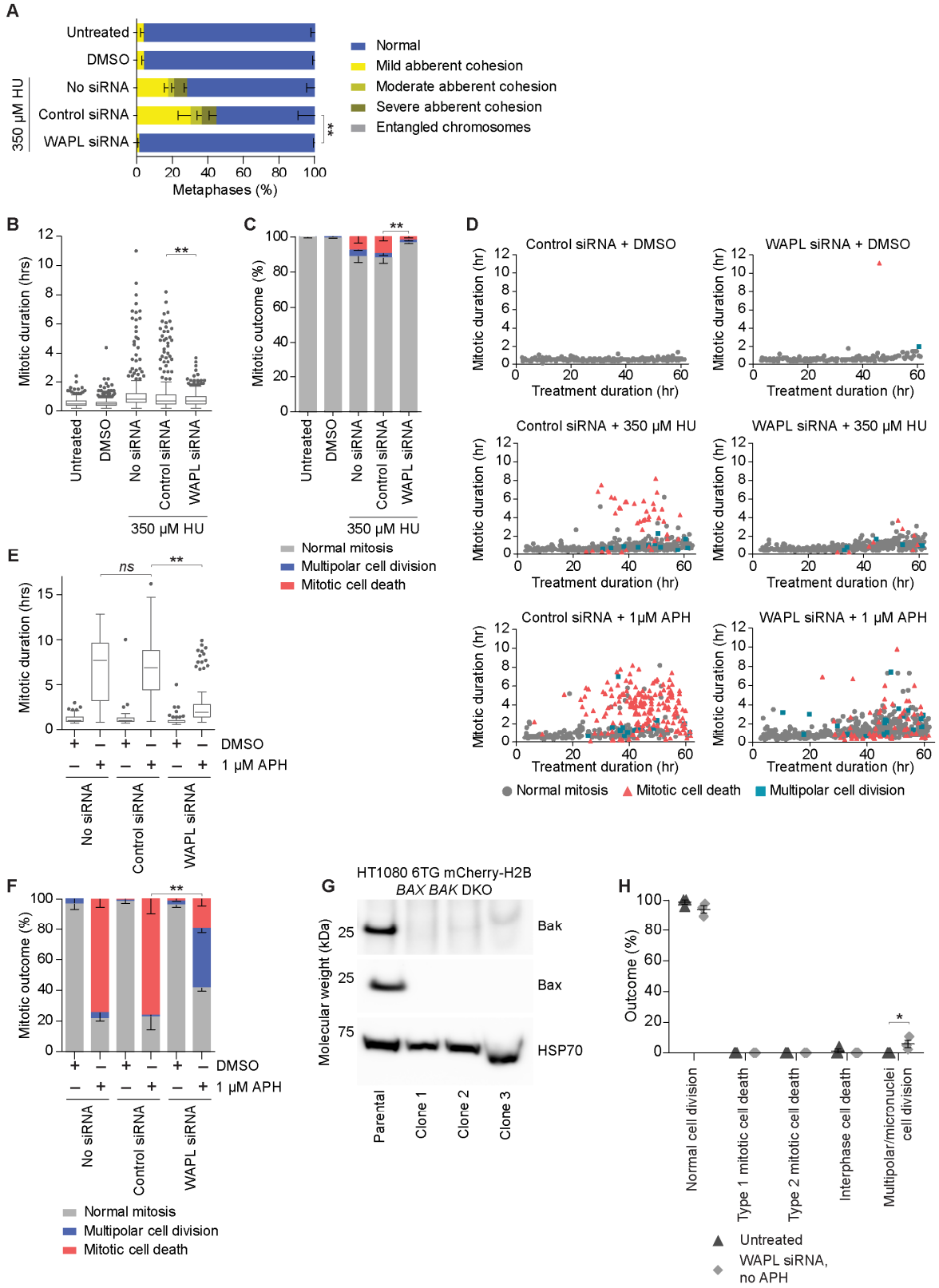
A
Untreated
DMSO
No siRNA
Control siRNA
WAPL siRNA
350 μM HU
Metaphases (%)
Normal
Mild abberent cohesion
Moderate abberent cohesion
Severe abberent cohesion
Entangled chromosomes
B
Mitotic duration (hrs)
C
Mitotic outcome (%)
Normal mitosis
Multipolar cell division
Mitotic cell death
D
Control siRNA + DMSO
WAPL siRNA + DMSO
Control siRNA + 350 μM HU
WAPL siRNA + 350 μM HU
Control siRNA + 1μM APH
WAPL siRNA + 1 μM APH
Treatment duration (hr)
Mitotic duration (hr)
E
ns
DMSO
1 μM APH
F
G
HT1080 6TG mCherry-H2B
BAX BAK DKO
Molecular weight (kDa)
Bak
Bax
HSP70
Parental
Clone 1
Clone 2
Clone 3
H
Outcome (%)
Normal cell division
Type 1 mitotic cell death
Type 2 mitotic cell death
Interphase cell death
Multipolar/micronuclei cell division
Untreated
WAPL siRNA, no APH

Figure S5. WAPL depletion rescues cohesion fatigue, mitotic arrest, and mitotic cell death in cells treated with lethal doses of APH or HU, related to Figure 4.A) Quantitation of cohesion phenotypes depicted in Fig. 4B in HT1080 6TG cells treated with HU ± siRNA (mean ± s.e.m, n= 3 biological replicates scoring ≥ 180 chromosome spreads per condition, Fisher's Exact Test). B) Mitotic duration of HT1080 6TG cells treated with HU ± siRNA (three biological replicates scoring ≥ 413 mitoses per condition are compiled into a Tukey box plot, Mann-Whitney test). C) Mitotic outcome of the cells in (B)(mean ± s.e.m., n = 3 biological replicates, Fisher's Exact Test). D) Two-dimensional representation of mitotic duration and outcome of the data in Fig. 4H, I and S5B, C). E) Mitotic duration of HeLa cells treated with DMSO and APH ± control or WAPL siRNA (three biological replicates scoring ≥ 43 mitoses per replicate are compiled into a Tukey box plot, Mann-Whitney test). F) Mitotic outcome of the cells in (E)(mean ± s.e.m., n = 3 biological replicates, Fisher's Exact Test). G) Western blot of HT1080 6TG-H2B mCherry parental and *BAX BAK* DKO clones. H) Mitotic outcome of WAPL depleted HT1080 6TG H2B-mCherry cells in the absence of APH (mean ± s.e.m., n = 3 biological replicates biological scoring ≥ 111 mitoses per condition). For all panels, *ns* = not significant, *p < 0.05, **p < 0.01.

Figure S6

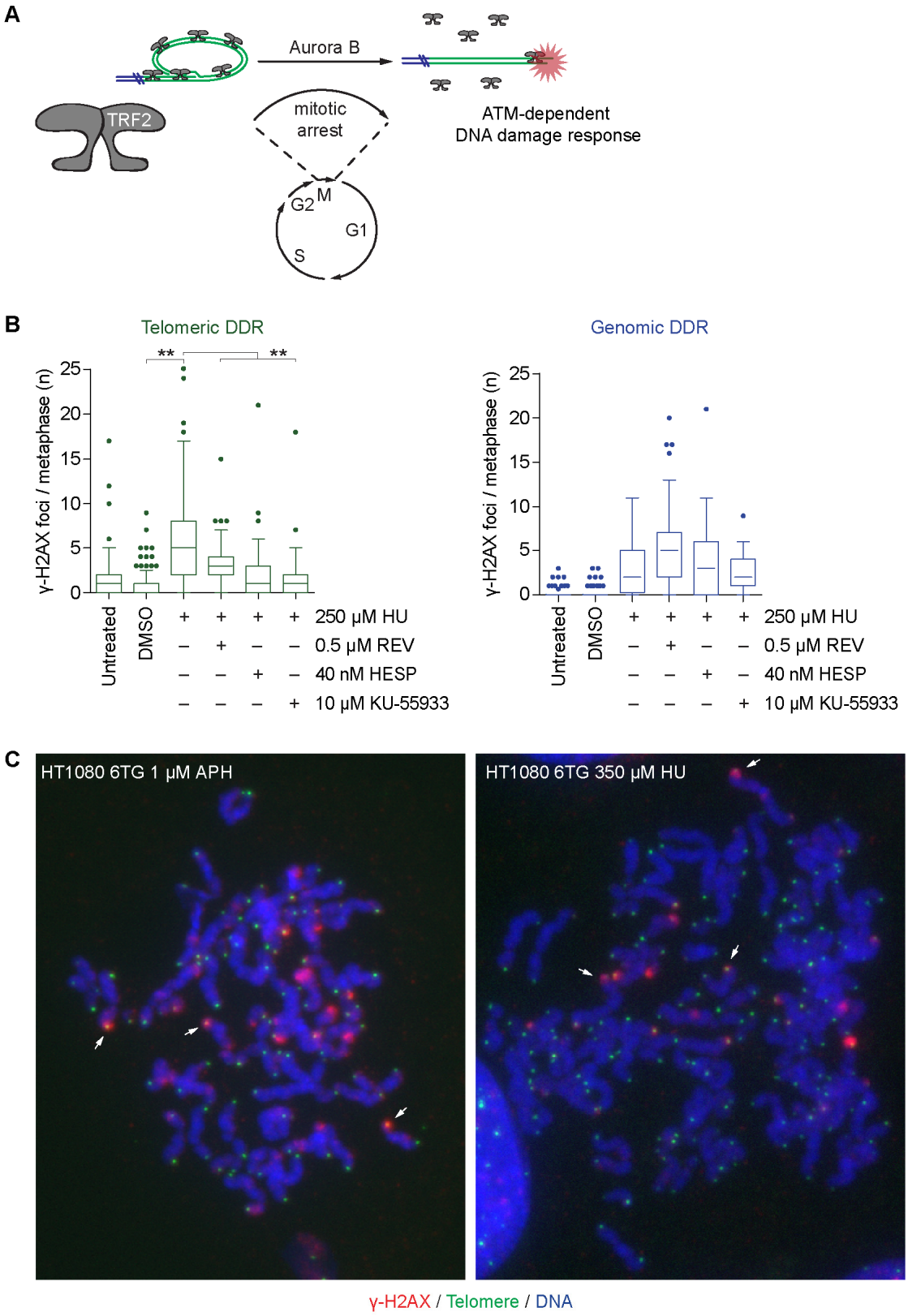
A
Aurora B
TRF2
mitotic arrest
ATM-dependent DNA damage response
G2
M
G1
S
B
Telomeric DDR
Genomic DDR
γ-H2AX foci / metaphase (n)
**
Untreated
DMSO
250 μM HU
0.5 μM REV
40 nM HESP
10 μM KU-55933
C
HT1080 6TG 1 μM APH
HT1080 6TG 350 μM HU
γ-H2AX / Telomere / DNA

Figure S6. The telomere DDR induced by lethal replication stress is dependent on mitotic arrest, Aurora B, and ATM, related to Figure 5. A) Graphical depiction of non-canonical, mitotic arrest-dependent telomere deprotection (Hayashi et al., 2012; Van Ly et al., 2018). B) Quantitation of telomeric and genomic DDR foci in HT1080 6TG cells treated with HU ± REV, Hesperidin (HESP), or KU-55933 (three biological replicates scoring $n \geq 37$ chromosome spreads per replicate are compiled in a Tukey box plot, Mann-Whitney test, $^{**}p < 0.01$). C) Representative image of cytocentrifuged chromosome spreads from APH or HU treated HT1080 6TG cells displaying telomere DDR foci and separated sister chromatids. Examples of telomere DDR foci on separated sister chromatids are indicated by the white arrows. Samples are stained with DAPI (blue), γ-H2AX IF (red) and telomere PNA (green).

Figure S7

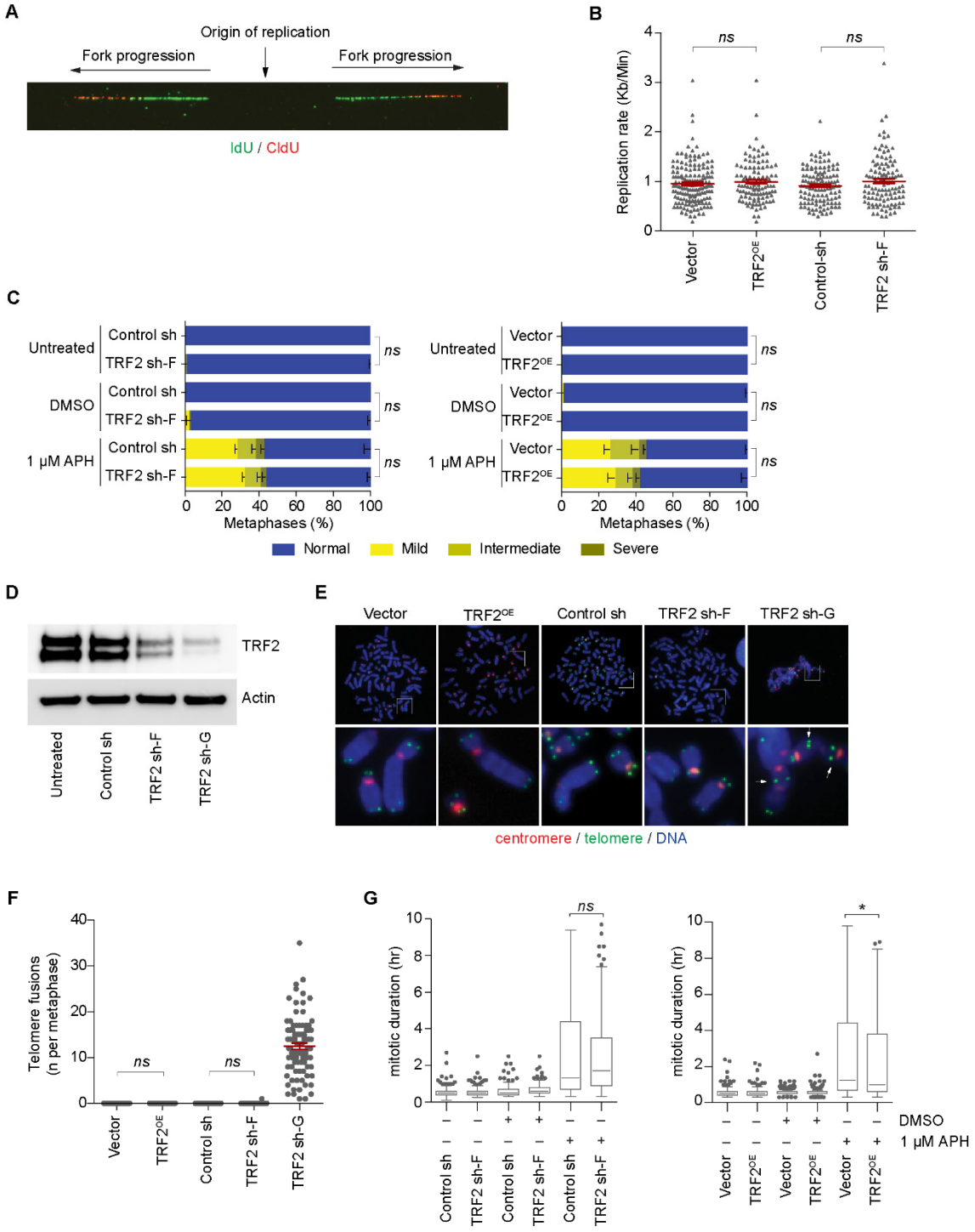
A
Origin of replication
Fork progression
Fork progression
IdU / CldU
B
Replication rate (Kb/Min)
ns
ns
Vector
TRF2OE
Control-sh
TRF2 sh-F
C
Untreated
DMSO
1 μM APH
Control sh
TRF2 sh-F
Vector
TRF2OE
ns
Metaphases (%)
Normal
Mild
Intermediate
Severe
D
TRF2
Actin
Untreated
Control sh
TRF2 sh-F
TRF2 sh-G
E
Vector
TRF2OE
Control sh
TRF2 sh-F
TRF2 sh-G
centromere / telomere / DNA
F
Telomere fusions (n per metaphase)
ns
ns
Vector
TRF2OE
Control sh
TRF2 sh-F
TRF2 sh-G
G
mitotic duration (hr)
ns
*
DMSO
1 μM APH
Control sh
TRF2 sh-F
Vector
TRF2OE

Figure S7. TRF2 sh-F and TRF2^{OE} do not impact genomic DNA replication rates, induce telomere fusions, or impact cohesion status, related to Figure 6. A) Representative image of chromatin fiber analysis to measure replication rates. B) Genomic DNA Replication rates in HT1080 6TG control, TRF2 sh-F, and TRF2^{OE} (all replication forks from two biological replicates are compiled into a dot plot, n ≥ *109* total forks measured per condition, mean ± s.e.m., Student's t-test). C) Quantitation of cohesion phenotypes as shown in Fig. 4B in HT1080 6TG cells transduced with the indicated vectors, treated with DMSO or APH (mean ± s.e.m of n = 3 experiments scoring ≥ 50 chromosome spread per replicate, Fisher's Exact Test). D) Western blots of whole cell extracts from HT1080 6TG cells transduced with TRF2 sh-F and the more effective TRF2 sh-G (Cesare et al., 2013). E) Representative cytogenetic chromosome spreads from HT1080 6TG cells transduced with the indicated vectors. Telomere-telomere fusions are indicted by arrows in TRF2 sh-G. F) Quantitation of telomere-telomere fusions from the conditions in (E) (three biological replicates scoring ≥ 30 mitotic spreads per replicate are compiled into a dot plot, mean ± s.e.m., Mann-Whitney test). G) Mitotic duration of HT1080 6TG control, TRF2 sh-F, and TRF2^{OE} cells treated with DMSO or APH (three biological replicates scoring n ≥ 267 mitoses per condition are compiled in a Tukey box plot, Mann-Whitney test). For all panels, ns = not significant, * $p < 0.05$.

Movie S1: Lethal replication stress induces mitotic death, related to Figure 1. Live cell imaging of HT1080 6TG cells treated with DMSO or 1 μM APH. Imaging duration is shown in the top left corner as (day:hr). Some examples of mitotic cell death events are indicated with a red “>” symbol.

Movie S2: Lethal replication stress induces mitotic death in the immediately following mitosis, related to Figure 2. Live cell imaging of HT1080 6TG FUCCI cells (Sakaue-Sawano et al. 2008) treated with DMSO or APH at t=0 hours. G1 phase cells are indicated by mCherry-hCdt1(30/120) stability and S/G2 phase cells by mVenus-hGeminin (1/110) stability. Duration of live cell imaging was shown on the top left corner of the movie (day:hr). Some examples of mitotic cell death events are indicated with a yellow “>”.

Movie S3: Two types of mitotic cell death are induced by replication stress, related to Figure 3. Spinning disk confocal live cell imaging of HT1080 6TG H2B-mCherry cells treated with 1 μM APH. Brightfield image was captured with differential interference contrast. Examples of Type 1 and Type 2 mitotic death are indicated.